American Mineralogist, Volume 98, pages 2115–2131, 2013

Medium-range order in disordered K-feldspars by multinuclear NMR

Luis Sánchez-Muñoz[1,*], Jesús Sanz[2], Isabel Sobrados[2] and Zhehong Gan[3]

[1]Instituto de Cerámica y Vidrio (CSIC), Kelsen 5, 28049 Madrid, Spain
[2]Instituto Ciencia de Materiales de Madrid (CSIC), Sor Juana Inés de la Cruz 3, 28049 Madrid, Spain
[3]National High Magnetic Field Laboratory, Florida State University, Tallahassee, Florida 32310, U.S.A.

Abstract

The structures of K-rich feldspar, $(K>Na)AlSi_3O_8$, are currently described as "ideal" crystals with periodic average structures from Bragg diffraction maxima obtained by reciprocal-space techniques. Polymorphism is explained by variable substitutional disorder of framework Si and Al cations in tetrahedral T sites, and positional disorder of cavity alkali cations in a single M site. Here, high-resolution magic angle spinning multinuclear magnetic resonance spectroscopy, leading to ^{29}Si, ^{27}Al, and ^{23}Na spectra at 9.4 as well as ^{27}Al, ^{39}K, and ^{23}Na spectra at 19.6 T, has been used to investigate the "real" structures along the order-disorder series of K-feldspar crystals. The "ideal" and "real" structure coincides only in the perfectly long-range ordered triclinic end-member of the low-microcline structure. Long-range disordered structures (either with monoclinic or triclinic symmetry by X-ray diffraction) show non-random disorder at the medium-range scale, triclinic-like distortions with four sets of T sites for framework atoms, two sets of M sites for alkali atoms, and Al-O-(K,Na) multi-site correlations by NMR spectroscopy. The K-feldspar structures can be described by a medium-range structure using the number of Al atoms per four-membered rings of tetrahedra, with "…-2-0-2-0-…" chains for microcline and orthoclase where the Al-occupancies $t_1O > t_2m > t_2O \approx t_1m$, and with "…-1-1-1-1-…" chains for valencianite and sanidine, in which $t_1O > t_2m \approx t_2O \approx t_1m$. Framework cations respect Loewenstein's rule (Al-O-Al avoidance), as well as some additional constraints of charge dispersion involving deficiency of Si atoms in Q^4 (4Si,0Al), (1Si,3Al), and (0Si,4Al) environments, constraints which are particularly strong in valencianite. These "real" structure features cannot be described by "ideal" structures owing to the lack of resolving power of the reciprocal-space techniques.

Keywords: K-feldspars, NMR, medium-range order, valencianite, order-disorder series

Introduction

Taylor's model of the archetypal structure of feldspars, induced from X-ray diffraction (XRD) data of *sanidine* (Taylor 1933; Taylor et al. 1934), suggests a monoclinic *C*2/*m* average symmetry if the framework of tetrahedra is idealized in a topology where the actual occupancy of T sites by Si and Al atoms is disregarded. The structure consists of three-dimensionally linked SiO_4 and AlO_4 tetrahedral units with two crystallographically non-equivalent tetrahedral sites, T_1 and T_2. The T sites form double crankshaft chains of four-member rings, replicated by mirrors parallel to (010). The alkali cations, located at a single M site inside an irregular cavity, ensure local electrostatic (ionic) neutrality. Immediately thereafter, Barth (1934) proposed an order-disorder relationship in the Si, Al distribution of the T sites to explain the structural diversity of K-feldspar in nature. Subsequent structural refinements (see Taylor 1965, for an early review) confirmed this hypothesis when site occupancies are correlated with mean T-O distances. As Si and Al atoms have similar X-ray scattering factors, it is impossible to refine site occupancies using X-ray data (Smith 1954). Sanidine was regarded as the high-temperature phase having completely random disorder, whereas *orthoclase* is seen to be partially ordered, with preferential segregation of Al atoms into the T_1 sites. Further Si/Al ordering can produce *microcline*, the low-temperature phase, with a lowering of the symmetry from *C*2/*m* to $C\bar{1}$, and a distortion of the unit-cell shape. The four T sites are labeled T_1O, T_1m, T_2O, and T_2m, with the Al atoms concentrated in the T_1O site and Si occupying three other sites (Megaw 1956). The Al-occupancies Al/(Al+Si) of the T sites, denoted as t_1O, t_1m, t_2O, and t_2m, allows the distinction between low microcline where $t_1O = 1.0$ and $t_1m = t_2O = t_2m = 0.0$ and intermediate microcline where $t_1O > t_1m > t_2O = t_2m$ (Ribbe 1983). It has been suggested that in the K-feldspars alkali atoms may have positional disorder along the order-disorder series, occupying slightly different positions around a single M site (see discussions by Megaw 1959 and Ribbe 1994, p. 21–24).

The description of crystal structures of K-feldspar in terms of time and space averages derived from Bragg diffractions in reciprocal-space techniques as "ideal" crystal structures, and the calculation of the degree of Si/Al order from T-O distances, have some weaknesses. That approach ignores the omnipresent X-ray diffuse scattering (Laves 1950) arising from structural modulations in orthoclase (McConnell 1965) and from intrinsic distortions of the framework due to different sizes of the AlO_4 and SiO_4 tetrahedra in sanidine (Pleger 1996). Random disorder in sanidine has not been demonstrated from average T-O distances

* E-mail: lsm@icv.csic.es

0003-004X/13/1112–2115$05.00/DOI: http://dx.doi.org/10.2138/am.2013.4448

induced by more recent determinations by XRD (Scambos et al. 1987; Kimata et al. 1996b) or neutron diffraction determinations (Brown et al. 1974). The lattice model for orthoclase with an average monoclinic symmetry is inconsistent with the local triclinic structure detected by other techniques (McLaren and Fitz Gerald 1987; Sánchez-Muñoz et al. 1998), as indicated by Laves and Goldsmith (1961). In addition, it is impossible to determine the exact Al occupancy of disordered Na-feldspars only on the basis of T-O bond distances, as the T sites have intrinsically different T-O bond lengths (Winter et al. 1979). This finding calls into question the usefulness of the approach in this family of minerals. The effect of alkali atoms (as only one M site is invoked), as well as possible strain effects (Eggleton and Buseck 1980) and the importance of the size of domains or twins to produce coherent diffraction (Ribbe 1983), also must be considered.

Available nuclear magnetic resonance (NMR) data for K-feldspars (Laves and Hafner 1962; Lippmaa et al. 1980; Smith et al. 1984; Kirkpatrick et al. 1985; Sherriff and Hartman 1985; Phillips et al. 1988; Zhou et al. 1994, 2001; Xiao et al. 1995; Sánchez-Muñoz et al. 1998, 2006a; Anbalagan et al. 2009) have supported the Si/Al order-disorder hypothesis partially. In particular, the NMR parameters of monoclinic K-feldspars do not correlate well with site occupancies determined by XRD (Xiao et al. 1995). Most of the available NMR studies have been performed at low fields using rather few samples, with limited characterization. The more disordered states have been investigated in much less detail than the ordered counterparts, owing to lack of sufficient spectral resolution. Data from the ^{29}Si and ^{27}Al spectra have not been correlated with those from the ^{39}K and ^{23}Na spectra along the order-disorder series. Moreover, disordered states having a triclinic symmetry (Chaison 1950; Laves 1950), termed *valencianite* by Akizuki and Sunagawa (1978), have been disregarded in most NMR investigations. In addition, ^{39}K spectra are difficult to obtain because of the low sensitivity and large quadrupolar coupling associated with highly asymmetric sites, particularly in disordered structures.

In this paper, we address the above questions by means of multinuclear NMR analysis at 9.4 and 19.6 T using specimens very similar to those characterized by X-ray methods in the literature to build up the conventional order-disorder model. The "real" structures are investigated to evaluate the hypotheses that: (1) the Si, Al occupancies in the framework T sites cannot be investigated independently of the distribution of alkali cation in the M split-sites in the cavity, (2) a quasi-triclinic local symmetry exists along the order-disorder series, and (3) the type of K-feldspar can be described with a specific polyatomic arrangement at the medium-range length scale, inaccessible with the resolving power of XRD techniques.

Table 1. The 33 specimens and samples of K-rich feldspar analyzed

K-feldspars	Chem. comp.	Locality	Origin	Source	K-feldspars
11924	$Or_{96.4}Ab_{3.6}$	Pikes Peak, Colorado, U.S.A.	1	1	MI
9544	$Or_{94.8}Ab_{5.2}$	Pikes Peak, Colorado, U.S.A.	2	2	MI
176	$Or_{98.0}Ab_{2.0}$	Colmenar Viejo, Madrid, Spain	3	3	MI
116	$Or_{92.9}Ab_{7.1}$	Colmenar Viejo, Madrid, Spain	3	3	MI
FB4	$Or_{91.1}Ab_{8.9}$	Belvis de Monroy, Cáceres, Spain	3	3	MI
5963	$Or_{93.5}Ab_{6.5}$	Valais, Switzerland	4	2	OR
1123	$Or_{92.8}Ab_{7.2}$	Valais, Switzerland	4	2	OR
ASGS	$Or_{90.6}Ab_{9.4}$	St. Gotthard, Switzerland	4	4	OR
K-ASGS	$Or_{100}Ab_{0}$	–	5	4	OR
AFTS	$Or_{90.3}Ab_{9.7}$	Tavebih, Sweden	4	4	OR
172-34	$Or_{87.0}Ab_{13.0}$	Rondadura, Switzerland	4	5	OR
OrtA2b	–	Salzburgo, Austria	4	4	OR
5368	–	Brinstentor, Switzerland	4	2	VA
1406	–	Guttanen, Switzerland	4	2	VA
382	$Or_{98.7}Ab_{1.3}$	Zillerthal, Tyrol, Austria	4	2	VA
1109	$Or_{97.6}Ab_{2.4}$	Zillerthal,Tyrol, Austria	4	2	VA
115-371	$Or_{96.6}Ab_{3.4}$	Marienberg, Germany	4	5	VA
5426	$Or_{97.5}Ab_{2.5}$	Pfunderthal, Tyrol, Austria	4	2	VA
AGM	$Or_{97.5}Ab_{2.5}$	Guanajuato, Mexico	4	4	VA
1407	$Or_{98.0}Ab_{2.0}$	Uri, Switzerland	4	2	VA?
RABB	–	Rabb Park, New Mexico, U.S.A.	6	3	SA
SBKS	$Or_{65.5}Ab_{30.2}An_{4.3}$	Baden, Kaisertuhl, Switzerland	7	4	SA
EU2	$Or_{62.3}Ab_{37.5}An_{1.5}$	Idaho, U.S.A.	7	3	SA
K-EU2	$Or_{100}Ab_{0.0}An_{0.0}$	–	5	3	SA
SSNI	–	Mt. Somma, Napoles, Italy	7	4	SA
SANCS1	–	Konstenblutten, Czech Republic	7	4	SA
SEE	$Or_{79.9}Ab_{16.2}An_{4.1}$	Los Lobos, Almería, Spain	7	4	SA
SVNI-1	$Or_{69.4}Ab_{28.8}An_{1.8}$	Mt. Vesuvius, Italy	7	4	SA
SVNI-2	$Or_{72.3}Ab_{25.9}An_{1.7}$	Mt. Vesuvius, Italy	7	4	SA
713r	$Or_{78.7}Ab_{21.3}$	Eifel, Germany	7	5	SA
*K-713r**	$Or_{100}Ab_{0.0}$	–	5,8	5	SA
7294	$Or_{100}Ab_{0.0}$	–	9	–	SA
CLBR	$Or_{2.9}Ab_{97.1}$	Golconda III, MG, Brazil	10	3	AB

Notes: Origin: (1) "White cap" or untwinned single-crystal microcline overgrowth on amazonite in a miarolitic pegmatite, Pikes Peak batholith (CO, U.S.A.). (2) Amazonite from a miarolitic pegmatite, also from Pikes Peak batholith. (3) Sample formed from fluids that fill the fractures and pockets in granitic pegmatites. (4) Transparent homogeneous morphological units of adularia habit from hydrothermal veins. (5) Synthetic product by ion-exchange experiments of specimens with KBr. (6) Subvolcanic pegmatite. (7) Single crystals separated from volcanic rocks. (8) Sample artificially disordered by thermal annealing at 1050 °C for 7 days. (9) Specimen synthesized at ISTO from a gel with pure $KAlSi_3O_8$ composition that was crystallized at 725 °C and 3 kbars for 168 h in hydrothermal conditions. (10) Albite with the cleavelandite habit from a pocket in a granitic pegmatite in Governador Valadares (MG, Brazil). Sources: (1) Ray Berry's collection; (2) Collected from Museo Geo-Minero, IGME, Madrid, Spain; (3) Collected by us at their original locality; (4) Collected from Museo Nacional de Ciencias Naturales de Madrid, CSIC, Spain. (5) Collected from Museé d'Histoire Naturelle de Paris (France). MI = microcline, OR = orthoclase, VA = valencianite, SA = sanidine, and AB = albite. Chemical compositions were obtained by EMPA.

THE K-FELDSPARS

Table 1 indicates the chemical composition, provenance, and host of the 33 natural specimens and synthetic samples of feldspars used in this work, including selected K-feldspar specimens well known in literature, a sample with stoichiometric $KAlSi_3O_8$ composition from hydrothermal crystallization at high temperatures and high pressure (sample *7294*), and three samples from ion-exchanged experiments using previous natural specimens as starting materials to obtain K-feldspar with composition close to $KAlSi_3O_8$ in a range of order-disorder states (samples *K-ASGS*, *K-EU2*, and *K-713r**). A crystal of Na-feldspar (specimen *CLBR*) was included. Most specimens are gem-quality materials in terms of transparency and uniformity at the optical scale, and display a single structural state in their XRD patterns. The terms used in this work include the recommendations of the International Mineralogical Association (IMA) to designate mineral species (Barth 1934), including microcline (MI), orthoclase (OR), and sanidine (SA). However, the term "valencianite" (VA) is needed to refer to some K-feldspar samples that cannot be labeled with the previous names; see Smith (1974) for an extended review of nomenclature.

Microcline

Specimen *11924* is close to that used by Blasi et al. (1984a) for the structure determination of the low-microcline end-member. Specimen *9544* has a XRD pattern very close to that of low microcline but shows regular albite-pericline twinning at both the optical and transmission electron microscopy (TEM) scales (Sánchez-Muñoz et al. 2012). Specimens *176* and *116* show heterogeneous optical extinction and "irregular twinning" (as described by Bambauer et al. 1989) at the TEM scale (Sánchez-Muñoz et al. 2006a). They correspond to the intermediate microcline XRD variety of Ribbe (1983). Specimen *FB*4 shows a heterogeneous diffraction pattern with broad (*hkl*), (*hk*0), and (0*kl*) peaks, indicating a triclinic structure with low obliquity.

Orthoclase

Orthoclase can form from high-temperature precursor like sanidine (normally with a high content of Na in solid solution), or at much lower temperatures in hydrothermal veins as crystals of adularia (with lower Na contents in solid solution). Because exsolution of the original feldspars takes place simultaneously with local ordering during slow cooling, a low-Na content reduces the contribution of Na-feldspar impurities to the K-feldspar spectra, improving the experimental resolution. Thus, crystals of adularia were selected instead of plutonic or metamorphic grains. The typical "tweed" pattern in our specimens (Table 1) and the associated orthogonal diffuse streaks in the [001] zone axis of selected-area electron diffraction (SAED) patterns, were studied by TEM by Sánchez-Muñoz et al. (1998), including the specimen *ASGS* from Saint Gotthard, Switzerland, similar to that originally studied by McConnell (1965), in which the tweed pattern was first noted. Our orthoclase specimens have a higher Na content in solid solution than the valencianite specimens, and negligible content of the anorthite component.

Valencianite

Specimens of valencianite are defined by the characteristics described in Chaison (1950), Laves (1950), and Akizuki and Sunagawa (1978): triclinic symmetry with low obliquity on the basis of optical and diffractometric data, very low-Na content in solid solution (Table 1), and the lack of tweed or twin microstructures at the TEM scale, as well as absence of diffuse streaks in SAED patterns. This variant indicates a particularly low temperature of crystallization, and thus, the triclinic character must be formed during crystallization at a temperature lower than the monoclinic-triclinic transition. In contrast, microcline almost invariably shows some residual twinning from the phase transformation of a monoclinic high-temperature precursor. Specimen *AGM*, from "Valenciana mine" in Guanajuato, Mexico, is very uniform and has the highest obliquity ($\gamma = 89.74°$) of our specimens. Specimen *1407* can be considered valencianite on the basis of chemical and microstructural features (as well as from the NMR data), but no peak splitting in (*hkl*), (*hk*0), and (0*kl*) reflections was detected. This specimen is therefore similar to adularia from Hishikari, Japan (Zhou et al. 2001).

Sanidine

The specimens used in this work are single crystals separated from glass material of felsic volcanic rocks, except specimen *RABB*, from a subvolcanic granitic pegmatite (O'Brient 1986; Keefer and Brown 1978). Specimens *RABB* and *SBKS* have well developed submicroscopic albite films from partial exsolution. The other specimens of sanidine do not show any evidence of exsolution. Additional features of specimen *EU*2 can be found in Sánchez-Muñoz et al. (2007). Specimens *SVNI*-1 and *SVNI*-2 are analogous to those used by W.H. Taylor in 1933 in the first X-ray determination of the structure of sanidine. Specimen *713r* is also comparable to that used in some other crystal-structure determinations (Brown et al. 1974; Kimata et al. 1996a and 1996b).

Synthetic samples

Ion-exchange experiments were conducted with orthoclase *ASGS* and sanidine *EU*2 to obtain samples with pure $KAlSi_3O_8$ composition as *K-ASGS* and *K-EU*2. Because valencianite invariably has a low content of Na in solid solution, no ion-exchange experiments were done in this case. Fine powders of the selected specimens were mixed with molten KBr at 825 °C for 30 h. In addition, the same experiments were performed at higher temperatures for specimen *713r* to obtain sample *K-713r** at 1050 °C for 15 h. In all cases, the ion-exchange products showed XRD pattern compatible with a monoclinic structure, as the original material had, i.e., no departure in the monoclinic symmetry was detected by XRD because of ion-exchange experiments. Sample *7294* was synthesized at 725 °C and 3 kbars for 168 h from a H_2O-oversaturated melt of $KAlSi_3O_8$ composition and with KF and AlF_3 additions as mineralizers, in the Institute des Sciences de la Terre d'Orléans (CNRS, France), with the help of François Delbove.

EXPERIMENTAL METHODS

Chemical analysis

Spatially resolved quantitative chemical analysis of the major elements Si, Al, Na, K, and Ca were performed by electron microprobe analysis (EMPA). We carried out an average of five or six analyses per sample, using a point-counting technique to obtain information on the chemical homogeneity, in a SX-50 instrument by Olivier Rouer in Institute des Sciences de la Terre d'Orléans (ISTO) in CNRS (France). Natural K-rich and Na-feldspars as well as synthetic pure K- and Na-feldspars

(also synthesized at ISTO) were used as chemical standards, which were previously analyzed by the electron probe in several experimental conditions to get the maximum signal and minimum loss of Na. The spot diameter of the probe was ca. 1 µm. The final operating conditions were 15 kV and 25 nA. A ZAF software was used for the correction of the matrix effects. The chemical compositions were expressed as $Or_xAb_yAn_z$ (x+y+z = 100) (Table 1), with Or, Ab, and An expressing the molar content of $KAlSi_3O_8$, $NaAlSi_3O_8$, and $CaAl_2Si_2O_8$ components in solid solution. Only some specimens of sanidine show an appreciable Ca content.

Nuclear magnetic resonance

High-resolution ^{29}Si, ^{27}Al, and ^{23}Na magic angle spinning (MAS) NMR spectra were recorded at 79.49, 104.23, and 105.80 MHz (9.4 T magnetic field), by spinning the sample at the magic angle (54°44′) using a Bruker Avance 400 spectrometer equipped with a Fourier transform unit of the Instituto de Ciencia de Materiales de Madrid (CSIC) in Spain. The samples were spun in the range of 4000 to 20 000 Hz. The pulse lengths are 4, 2, and 2 µs; the recycle delays are 1800, 5, and 5 s; and the *rf* field are 60, 50, and 50 kHz, respectively for the ^{29}Si, ^{27}Al, and ^{23}Na nuclei, to get a maximum in the intensity of the experimental signal. Recycle-delay times for ^{29}Si spectra were tested for values between 60 and 1800 s in samples with different structural state and chemical compositions to avoid saturation effects in the ^{29}Si signals. Crystals from volcanic rocks show iron impurities in T sites at the parts per million scale, and a recycle time of 60 s was sufficient to obtain the ^{29}Si spectra. However, crystals formed at low temperatures do not show such paramagnetic impurities, and the best results were obtained for 1800 s relaxation delays. Therefore, to get appropriate comparison of the NMR spectra of the whole set of specimens and samples, 1800 s were used in all cases. The number of accumulations was 200 for Al, and 50 for Si and Na signals.

High-resolution ^{27}Al, ^{39}K, and ^{23}Na spectra magic angle spinning (MAS) NMR spectra were acquired also at 216.14, 38.89, and 219.42 MHz (19.6 T magnetic field), using an 830 MHz Bruker DRX NMR spectrometer at the National High Magnetic Field Laboratory (NHMFL) in Tallahassee, Florida. Spectra were recorded with a 4 mm home-built MAS probe at 10 kHz sample spinning. The pulse lengths are 0.75, 2, and 0.75 µs; the recycle delays are 2, 1, and 2 s; and the *rf* field are 70, 50, and 70 kHz, respectively for the ^{27}Al, ^{31}K, and ^{23}Na nuclei. The number of accumulations was 128 for ^{27}Al, and 1024 for ^{23}Na signals, and between 3712 scans (e.g., in specimen *116*) and 65 536 scans (e.g., in specimen *11924*) for ^{39}K.

Chemical shifts are reported in parts per million relative to external references at room temperature, specifically, to tetramethylsilane (TMS) for ^{29}Si, 1 M $AlCl_3$ aqueous solution for ^{27}Al, KBr for ^{39}K, and 1 M NaCl aqueous solution for ^{23}Na spectra. The mean error in the measured chemical shift of the NMR components was ~1 ppm for ^{29}Si, ^{27}Al, and ^{23}Na spectra, and ca. 10 ppm for ^{39}K spectra. Kaolinite, KBr, and Na_2HPO_4 were used as samples to calibrate the pulse widths for ^{27}Al, ^{39}K, and ^{23}Na, respectively.

The ^{29}Si signals (I = 1/2) were analyzed by comparison of experimental curves with simulated profiles using Gaussian components for the different crystallographic sites in distinct crystallochemical environments, with identical line widths and variable intensities related to the Si, Al occupancies of the T sites. There is no physical basis for assigning identical line widths to geometrically different sites in distinct chemical environments in the simulation of a single spectrum. However, we limited the number of fit parameters to a minimum, mainly chemical shifts and relative areas (or intensities) in the deconvolution of spectra. Additional difficulties come from the lack of information about chemical shifts for the Al ↔ Si substitutions in the second-coordination sphere, as well as the effect of K and Na atoms. Finally, we chose 4.85 ppm as a shift between Si(nAl) and Si([n+1] Al) peaks for all the simulations, a value compatible with other NMR studies of aluminosilicates with tectosilicate structures (e.g., Klinowski et al. 1982; Phillips and Kirkpatrick 1995; Xiao et al. 1995); its use allows the reproduction of the main spectral features of most K-feldspars.

The ^{27}Al, ^{39}K, and ^{23}Na NMR spectra were fitted with Bruker WINFIT and DM2011 (Massiot et al. 2002) software, to calculate the quadrupolar constants C_Q, the asymmetry factor η, and the line width of each component. Where the second-order quadrupolar effects are visible in the central transition, the chemical shift and the quadrupolar constant were determined from the fitting of the central transition profile. An estimation of the second-order quadrupolar correction to the chemical shift was obtained from the displacement of the center of gravity with external magnetic field from 9.4 to 19.6 T, using the SORGE diagram of Massiot et al. (1995). Where a single magnetic field was used and the second-order quadrupolar effects are not visible, the values of chemical shift cannot be determined.

X-ray diffraction patterns

The feldspars were studied by powder XRD patterns to identify the mineral species and varieties using an INEL CPS 120 instrument with Co$K\alpha_1$ radiation at 30 kV and 25 mA, with Si as an internal standard. Spectra were recorded at 0.3°/min with 2° slits on samples placed in turning glass capillary tubes with a diameter of 0.50 mm. With these patterns, the K-feldspars were identified (last column in Table 1) using XRD data from Blasi (1984), Blasi et al. (1984b), and Kroll et al. (1986).

Eleven specimens and samples of K-feldspars, belonging to one of the four types listed in Table 1, were selected to obtain unit-cell parameters using Rietveld refinement by means of the whole-pattern decomposition or profile-matching method (Table 2). The procedure is known as the Le Bail fitting (Le Bail et al. 1988; Rodriguez-Carvajal 1993), using the FULLPROF (Rodríguez-Carvajal 2001) and the WinPLOTR software (Roisnel and Rodriguez-Carvajal 2001). This method does not require any structural information except approximate unit-cell dimensions and resolution parameters. These particular patterns were obtained using a Philips PANalytical X'Pert PRO MPD Alfa1 diffractometer. Incident X-ray radiation was produced with a PW 3373/10 Cu LFF DK175180 instrument, with Cu$K\alpha_1$ radiation at 45 kV and 40 mA. XRD patterns were recorded between 4.0 and 130.0 °2θ, with a step size of 0.008° in a continuous scan mode, using a Ge monochromator (Inc Beam 1xGe111 Cu/Co), a X'Celerator RTMS-type detector, and a X'Pert program for data collection. Cell parameters were used to obtain order parameters, specifically Σt_1 ($t_1O + t_1m$) and Σt_2 ($t_2O + t_2m$) using formulas of Kroll and Ribbe (1987), to classify the K-feldspar specimens and samples as XRD varieties (Ribbe 1983). With this study, the IMA-approved mineral species (Table 1) were correlated with the XRD varieties (Table 2), except for "valencianite" specimens, in which the triclinic character derived from cell angles is not correlated with order-disorder based on unit-cell dimensions (see Smith 1974, for additional discussion about K-feldspar nomenclature). Hence, as a whole, these materials do not correlate well with the paradigmatic sequence of K-feldspar formation on cooling, in the sequence sanidine → orthoclase → microcline. In particular, specimen *AGM* has the sharpest peak splitting from obvious triclinic character and shows the most disordered structure on the basis of cell dimensions, with the lowest Σt_1 value (Table 2). On the other hand, specimen *1407*, with a relatively high Σt_1 value, shows no evidence of the splitting of peaks as expected from a sharp monoclinic lattice.

TABLE 2. Lattice cell parameters, Si/Al order parameters, and K-feldspar varieties from XRD patterns

Materials	*a*	*b*	*c*	α	β	γ	*V*	Σt_1	Δt_1	XRD varieties
11924	8.582(1)	12.964(1)	7.225(1)	90.65(1)	115.93(1)	87,67(1)	722.3(1)	0.99(1)	1.00(1)	LM
9544	8.581(1)	12.965(1)	7.222(1)	90.64(1)	115.94(1)	87.68(1)	721.9(1)	0.97(1)	0.99(1)	LM
176	8.587(1)	12.966(1)	7.218(1)	90.50(1)	116.00(1)	88.09(1)	721.9(1)	0.93(1)	0.82(1)	IM
1123	8.560(1)	12.972(1)	7.210(1)	90.00	116.02(1)	90.00	719.4(1)	0.89(1)	0.00	OR
AFTS	8.564(1)	12.990(1)	7.204(1)	90.00	115.99(1)	90.00	720.4(1)	0.80(1)	0.00	OR
5368	8.581(1)	13.006(1)	7.199(1)	90.03(1)	116.03(1)	89.86(1)	721.9(1)	0.71(1)	0.06(1)	nc
1406	8.576(1)	13.004(1)	7.190(1)	90.03(1)	116.02(1)	89.85(1)	720.6(1)	0.68(1)	0.06(1)	nc
AGM	8.594(1)	13.024(1)	7.177(1)	90.06(1)	116.07(1)	89.74(1)	721.6(1)	0.54(1)	0.11(1)	nc
1407	8.593(1)	13.000(1)	7.192(1)	90.00	116.02(1)	90.00	722.0(1)	0.71(1)	0.00	LS
*K-713r**	8.605(1)	13.041(1)	7.184(1)	90.00	115.99(1)	90.00	724.6(1)	0.55(1)	0.00	HS
EU2	8.433(1)	13.006(1)	7.170(1)	90.00	116.05(1)	90.00	706.5(1)	0.59(1)	0.00	HS

Notes: Σt_1 and Δt_1 values were calculated using the methods of Kroll and Ribbe (1987) from the cell parameters. XRD varieties are from Ribbe (1983): HS = high sanidine, LS = low sanidine, OR = orthoclase, IM = intermediate microcline, and LM = low microcline. Valencianite specimens with an X-ray pattern consistent with triclinic symmetry cannot be classified by using these terms (nc). Values in parentheses are estimated standard deviations in the last decimal place.

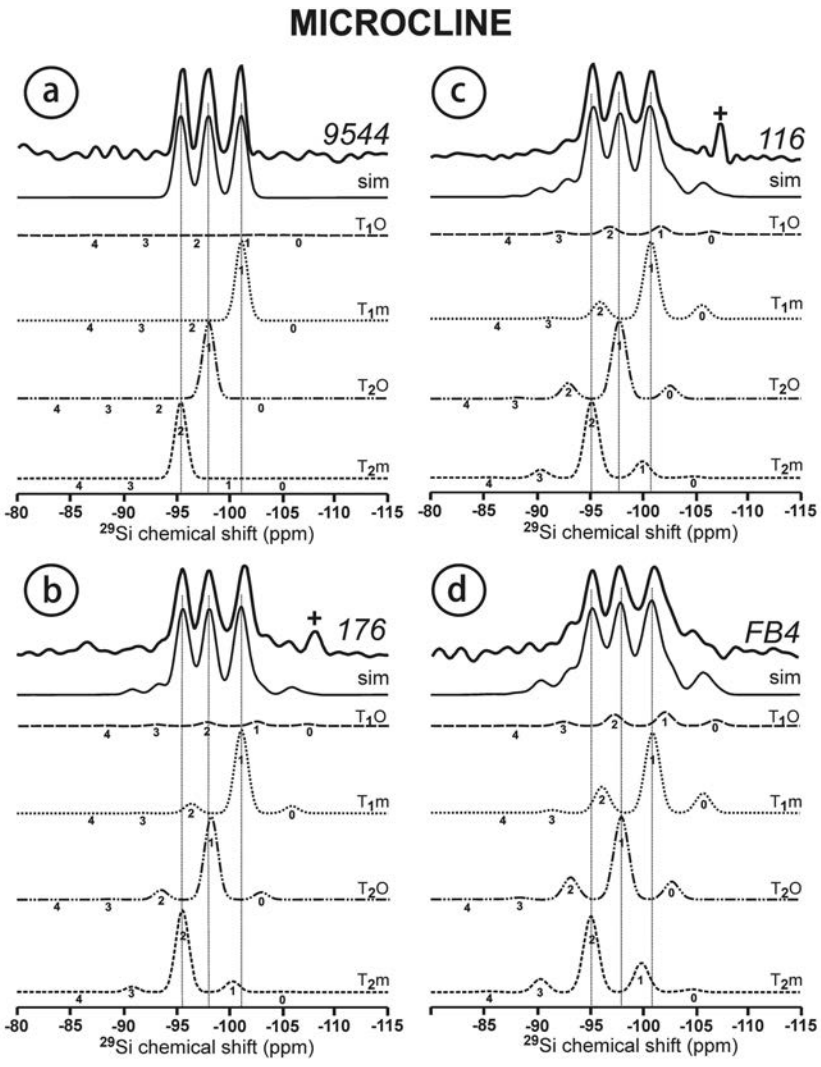

Figure 1. The ^{29}Si MAS NMR spectra of microcline at 9.4 T, with spectral simulations (sim) resulting from the additions of four components (T_1O, T_1m, T_2O, and T_2m), with five chemical environments as Si Q^4(nAl) for n = 0, 1, 2, 3, 4. (**a**) Specimen *9544*, (**b**) specimen *176*, (**c**) specimen *116*, and (**d**) specimen *FB4* (see Table 5[1] for relative intensities). Symbol "+" for the signal from quartz.

Results and spectral simulations

^{29}Si MAS NMR spectra

In Figures 1 to 4, we summarize representative ^{29}Si spectra of the K-feldspar samples studied. Tables 3 and 4 (and Tables 5 and 6 on deposit[1]) show the peak positions and intensities used in the spectral simulations of alternative models. In all cases, the specific intensities of peaks for each T site with the variable chemical environment were calculated assuming a fixed Si:Al ratio equal to 3:1 and Al-O-Al avoidance (Loewenstein's rule: Loewenstein 1954), using the expressions of Xiao et al. (1995), but in the following tetrahedral environments: the T_1O site is surrounded by 1 T_1m, 1 T_1O, and 2 T_2m sites; the T_1m by 1 T_1O, 1 T_2m, and 2 T_2O; the T_2O by 1 T_1O, 1 T_2m, and 2 T_1m; and finally the T_2m by 1 T_1m, 1 T_2O, and 2 T_1O. The chemical shift difference between the peaks for Si(nAl) and Si([n+1]Al) environments was assumed to be +4.85 ppm in all cases. The relationship between the peak intensity I_x in % and the Al occupancy t_x is given by $t_x = 1 - 3(I_x/100)$. With these basic assumptions, the main spectral features of most K-feldspars can be reasonably explained.

Two contrasting types of ^{29}Si spectra were observed. Microcline, orthoclase, valencianite, and sanidine (when it is close to the $KAlSi_3O_8$ composition, either from K→Na ion-exchange of natural Na-rich sanidine or by stoichiometric crystallization in hydrothermal experiments) have spectra with three maxima at –95.0 ± 0.3, –97.6 ± 0.3, and –100.8 ± 0.5 ppm, and some additional lateral shoulders (Figs. 1, 2, and 3). However, natural sanidine (Fig. 4) consist of two maxima at –96.5 ± 0.5 and –100.2 ± 0.4 ppm with some minor lateral shoulders in non-exsolved specimens (e.g., specimen *EU*2), whereas two maxima at –97.5

[1] Deposit item AM-13-1112, Tables 5–6. Deposit items are stored on the MSA web site and available via the American Mineralogist Table of Contents. Find the article in the table of contents at GSW (ammin.geoscienceworld.org) or MSA (www.minsocam.org), and then click on the deposit link.

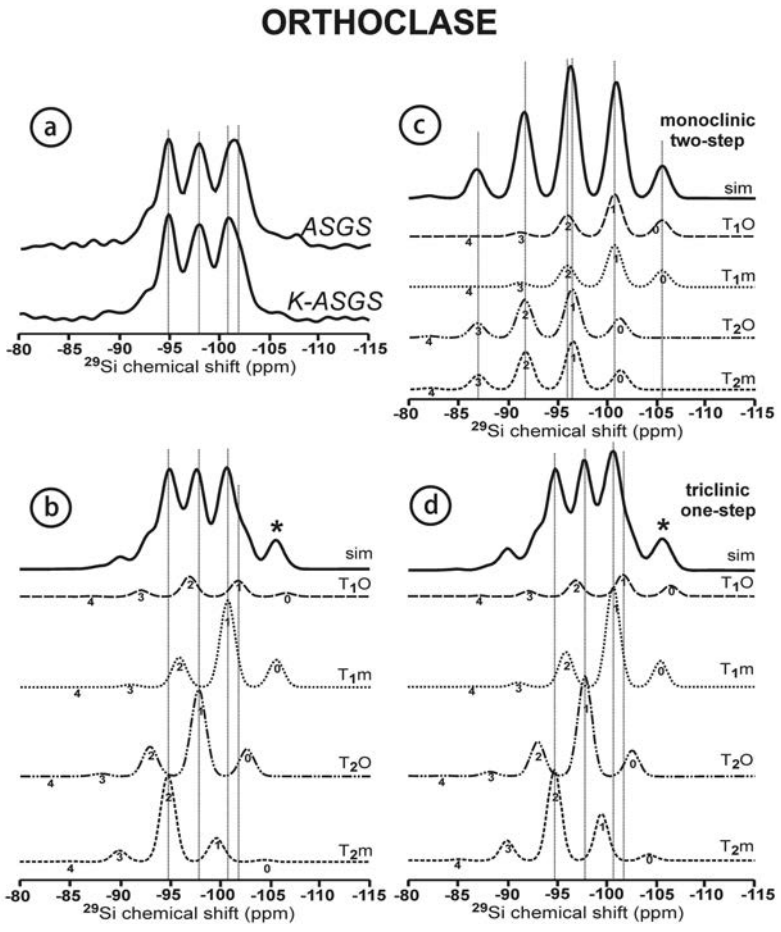

Figure 2. The ^{29}Si MAS NMR spectra of orthoclase at 9.4 T with spectral simulations as in Figure 1. (**a**) Spectrum in natural orthoclase (specimen *ASGS*) and its ion-exchanged product (sample *K-ASGS*). (**b**) Calculated spectrum for $t_1O = 0.7$, $t_1m = t_2O = 0.05$, $t_2m = 0.2$ (see Table 5[1] in supporting information online for relative intensities). (**c**) Calculated spectra for two-step orthoclase with monoclinic symmetry for $t_1O = t_1m = 0.4$ and $t_2O = t_2m = 0.1$. (**d**) Calculated spectra for one-step orthoclase with triclinic symmetry $t_1O = 0.7$ and $t_1m = t_2O = t_2m = 0.1$ and reduced local obliquity. Table 6[1] has the relative peak intensities for each model. Symbol "*" see text for explanation.

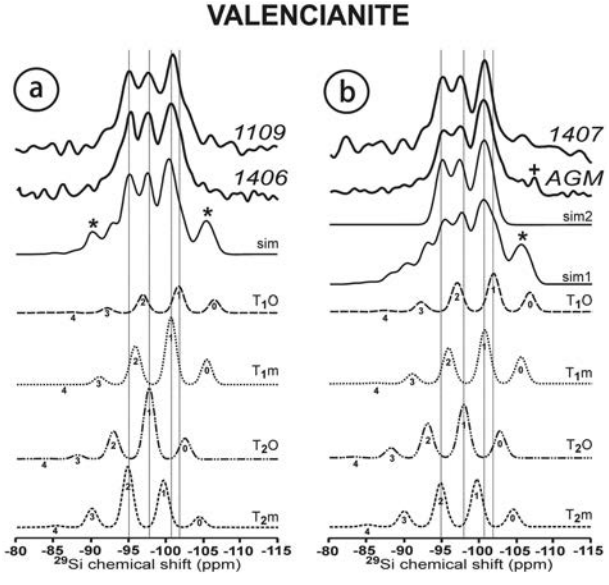

◄**Figure 3.** The ^{29}Si MAS NMR spectra of valencianite at 9.4 T with spectral simulations as in Figure 1. (**a**) Spectra from specimen *1109* and specimen *1406* in comparison with a calculated spectrum for a triclinic structure with $t_1O = 0.60$, $t_1m = 0.10$, $t_2O = 0.20$, and $t_2m = 0.10$. (**b**) Spectra from specimens *1407* and *AGM* in comparison with a calculated spectrum for a triclinic structure with $t_1O = 0.40$ and $t_1m = t_2O = t_2m = 0.20$. Sim1 and sim2 are built up using different intensities in Table 5[1]. Symbol "+" for the signal from quartz, and symbol "*" see text for explanation.

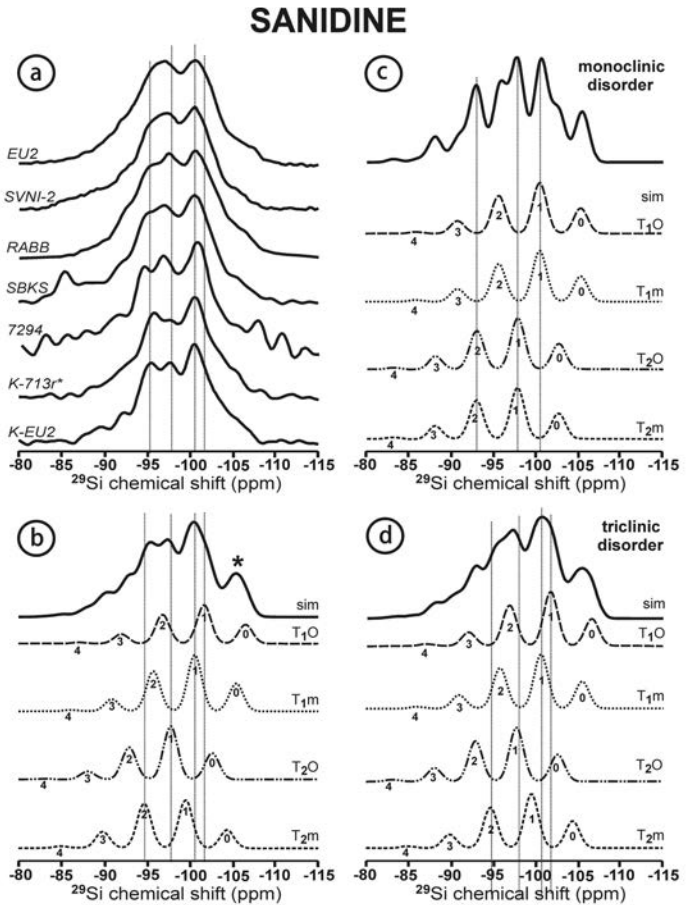

Figure 4. The ^{29}Si MAS NMR spectra of sanidine at 9.4 T with spectral simulations as in Figure 1. (**a**) Specimens *EU*2, *SVNI*-2, *RABB*, and *SBKS*, and samples *7294*, *K-713r**, and *K-EU2*. (**b**) Calculated spectrum for a sanidine ($t_1O = 0.40$, $t_1m = 0.15$, $t_2O = 0.25$, and $t_2m = 0.20$) with a triclinic structure but reduced local obliquity. (**c**) Calculated spectrum for strict monoclinic symmetry $t_1O = t_1m = t_2O = t_2m = 0.25$. (**d**) Calculated spectrum for triclinic symmetry with reduced obliquity and the same occupancies of **c**. Symbol "*" see text for explanation.

Table 3. NMR parameters from simulation of the ^{29}Si spectra

Specimens	*9544*	*176*	*116*	*FB4*	*K-ASGS*	*1406*	*AGM*		*K-EU2*
Line width	0.65	0.80	0.90	1.00	1.10	1.00	sim1 1.10	sim2 1.50	1.35
t_1O	1.00	0.89	0.78	0.74	0.70	0.60	0.40	0.40	0.40
t_1m	0.00	0.03	0.05	0.06	0.05	0.10	0.20	0.20	0.15
t_2O	0.00	0.03	0.06	0.09	0.05	0.20	0.20	0.20	0.25
t_2m	0.00	0.05	0.11	0.11	0.20	0.10	0.20	0.20	0.20
δT_1O (ppm)	–	–102.2	–102.2	–102.1	–101.8	–101.7	–101.7	–101.5	–101.7
δT_1m (ppm)	–100.9	–100.8	–100.8	–100.9	–100.7	–100.7	–100.6	–100.2	–100.6
δT_2O (ppm)	–97.8	–97.7	–97.7	–97.9	–97.8	–97.8	–97.8	–97.4	–97.8
δT_2m (ppm)	–95.2	–95.2	–95.2	–95.0	–94.9	–94.9	–94.7	–95.0	–94.7

Notes: The letter "t" lowercase is used for the Al content in the T sites, which are named with "T" uppercase. Specimen *AGM* has two spectral simulations: sim1 and sim2 (Fig. 3). δT_x values are given for the T_1O (3Si,1Al), T_1m (3Si,1Al), T_2O (3Si,1Al), and T_2m (2Al,2Si) sites.

± 0.3 and –100.5 ± 0.3 ppm with a well-developed shoulder at approximately –95.2 ppm, are found in specimens in which an exsolution-induced microtexture is developed (e.g., specimen *RABB*).

Figure 1 displays the ^{29}Si spectra of microcline specimens. The spectrum of specimen 9544 consist of three Gaussian peaks of equal intensity and width, attributed to Si atoms in T_2m (2Si,2Al) at –95.2 ppm, T_2O (3Si,1Al) at –97.2 ppm, and T_1m (3Si,1Al) at –100.9 ppm. This spectrum is consistent with the low-microcline structure as the fully ordered end-member of the order-disorder series, with Al atoms occupying only the T_1O site (Lippmaa et al. 1980; Smith et al. 1984; Kirkpatrick et al. 1985; Phillips et al. 1988; Xiao et al. 1995). If partial disorder exists, new signals from Si at T_1O and new chemical environments are generated as shown in three specimens of intermediate microcline (Figs. 1b–1d). These spectra were reasonably simulated with chemical shifts similar to those of the low microcline, and the signal from Si atoms in T_1O (3Si,1Al) at –102.2 ppm. This analysis suggests

TABLE 4. NMR parameters from simulation of the ^{27}Al, ^{39}K, and ^{23}Na spectra at 19.6 T

K-feldspar types		Microcline			Orthoclase	Valencianite		Sanidine	
Specimens		*11924*	*9544*	*116*	*1123*	*1406*	*AGM*	*K713r**	*EU2*
		Framework cations in tetrahedral T sites							
		^{27}Al at 19.6 T							
T_1	δ_{iso} (ppm)	–	59.2	59.8	60.3	60.6	60.7	60.8	61.0
	Em	–	50	65	80	85	85	80	95
	C_Q (kHz)	–	3150	3641	3650	3716	3664	4006	3932
	η	–	0.25	0.35	0.38	0.42	0.52	0.50	0.50
	Σt_1	–	~1.00	0.895	0.805	0.689	0.555	0.542	0.558
T_2	Position (ppm)	–	~61.1	61.1	61.0	61.4	61.8	61.6	61.7
	Width (ppm)	–	–	3.3	3.5	3.5	3.6	3.6	3.9
	Σt_2	–	~0.0	0.105	0.195	0.311	0.445	0.458	0.442
		Alkali cations in M sites at irregular cavities							
		^{39}K at 19.6 T							
M_1	δ_{iso} (ppm)	–65.2	–55.7	–60.5	–49.8	–62.5	–65.2	–73.2	–80.3
	Em	14	17	25	40	45	50	50	70
	C_Q (kHz)	1911	2032	1953	2101	2048	2151	1830	2037
	η	0.87	0.87	0.85	0.65	0.65	0.65	0.65	0.65
	Σm_1	1.00	~1.00	0.852	0.765	0.674	0.566	0.587	0.537
M_2	Position (ppm)	–	–	–90.0	–86.3	–90.2	–98.6	–95.2	–85.56
	Width (ppm)	–	–	62	63.7	62	72	57.2	74.8
	Σm_2	–	–	0.146	0.235	0.326	0.434	0.412	0.463
		^{23}Na at 19.6 T							
M_1	δ_{iso} (ppm)	–24.7	–24.9	–23.5	–22.6	–22.4	–21.9	–	–20.1
	Em	80	80	80	80	80	80	–	80
	C_Q (kHz)	1160	1146	1685	1993	2010	2051	–	2136
	η	0.70	0.70	0.60	0.60	0.60	0.65	–	0.60
	Σm_1 (%)	1.00	0.904	0.792	0.787	0.675	0.530	–	0.555
M_2	Position (ppm)	–	–24.7	–22.7	–22.0	–21.9	–21.0	–	–19.9
	Width (ppm)	–	1.5	2.5	3.4	5.4	6.8	–	5.4
	Σm_2	–	0.096	0.208	0.212	0.325	0.470	–	0.445

Notes: Estimated uncertainties in the chemical shifts are ±1 ppm for the ^{27}Al and ^{23}Na spectra, and 10 ppm for ^{39}K spectra. Uncertainties are 100 kHz in C_Q, and 0.2 in η parameter of ordered samples. Estimated uncertainties in cation occupancies are ±10%.

that Al atoms are mainly located at T_1O sites, with $t_1O > 0.73$ as expected from XRD data, but complemented with $t_2m > t_2O \approx t_1m$ values (Table 3), in contrast to conventional models from XRD data where $t_1m > t_2O \approx t_2m$ occupancies are indicated.

Surprisingly, orthoclase specimens have very similar spectra in all cases (Fig. 2a), consisting of three peaks with maxima at almost the same positions of microcline, and with analogous intensity (but the peak at –100.8 ppm has larger area than the other two peaks), as well as some minor lateral shoulders at –92.5 and –105.2 ppm. The ion-exchange experiments do not change the ^{29}Si spectra of orthoclase significantly (compare *ASGS* with *K-ASGS* in Fig. 2a). No indication of obliquity was found in the XRD pattern of sample *K-ASGS* after the ion-exchange experiments, as it was absent before the cation exchange. The spectral simulations compatible with the experimentally observed spectra of orthoclase (Fig. 2b) were obtained by considering the t_1O value to be between 0.70 and 0.80, a t_2m value between 0.10 and 0.20, t_2O and t_1m values between 0.05 and 0.10, and δ T_1O (3Si,1Al) = –101.7 ppm, δ T_2m (2Si,2Al) = –94.9 ppm (Table 3, and Table 5[1]). Our simulation of the orthoclase spectra shows that $t_2m > t_2O \approx t_1m$ is very characteristic of this structure. However, the signal from Si at T_1m (4Si,0Al) is invariably more developed in the simulations that in the original spectra, indicating that additional restrictions to that of the Loewenstein's rule must be at work, for instance some additional dispersion of charges reducing the development of (4Si,0Al) environment at the T_1m site (asterisk in Fig. 2). The ^{29}Si spectrum for a two-step monoclinic orthoclase was simulated in Figure 2c with a typical Si, Al distribution over two T sites with $t_1O = t_1m = 0.4$ and $t_2O = t_2m = 0.1$ (Table 6[1]), as generally suggested by XRD. In addition, the spectral simulation of the one-step triclinic orthoclase with $t_1O = 0.7$ and $t_1m = t_2O = t_2m = 0.1$ (Table 6[1]) is shown in Figure 2d. Both alternative models reproduce the experimental results more poorly than the simulations already suggested in Figure 2b, particularly if a monoclinic structure is considered.

Figure 3 exhibits the ^{29}Si spectra of the valencianite specimens, which are characterized mainly by the same three peaks of previous feldspars, however the peak at –100.7 ppm is broader and more inhomogeneous having almost double area and higher intensity than the other two peaks at –95.2 and –97.5 ppm, displaying also minor lateral signals at –90.1, –92.5, and –105.2 ppm. The spectra of the less disordered valencianite specimens can be simulated partially with t_1O values of about 0.6 and $t_2O > t_2m \approx t_1m$ (specimens *1406* and *1109*: Fig. 3a, Table 3). The broad peak with a maximum at about –105.2 ppm, formed by the addition of signals from Si at T_1O (4Si,0Al), T_1m (4Si,0Al), and T_2m (4Si,0Al), and that at –90.1 ppm, reflecting Si at T_2O and T_2m with a (1Si,3Al) environment (asterisk in Fig. 3), are much more developed in the simulations than in the experimental spectra. The more disordered valencianite specimens, as judged from NMR results (specimens *AGM* and *1407*), are shown in comparison with two simulated spectra for $t_1O = 0.4$ and $t_1m = t_2O = t_2m = 0.2$ (sim1 and sim2) in Figure 3b. The spectrum sim1 is constructed with all the possible Si Q^4 (nAl) environments for Si:Al = 3:1 and peak intensities complying Loewenstein's rule. However, spectrum sim2 considers only the four major sites compatible with the same Al occupancy, i.e., T_1O (3Si,1Al), T_1m (3Si,1Al), T_2O (3Si,1Al), and T_2m (2Si,2Al), for which the peak positions are close to the standard values in microcline and orthoclase, and a wider line width (see Table 3 for details). It is

clear that the experimental spectra are intermediate between these two cases, indicating that strong homogenization on the charge distribution occurs throughout the framework during growth of these distinctive disordered structures, at a low temperature.

Figure 4a shows the ^{29}Si NMR spectra of specimens *EU*2 and *SVNI*-2; both are very similar to the specimens studied by Taylor (1933) in that they have a high sodium content in solid solution (Table 1) as a consequence of a high temperature of crystallization from alkali-rich magmas in a volcanic environment. Their spectra show two maxima interpreted as corresponding to T_1 and T_2 sites in a monoclinic lattice (Kirkpatrick et al. 1985; Zhou et al. 1994; Anbalagan et al. 2009), as expected from Taylor's model. Where sanidine shows exsolution, the spectra have an additional shoulder at –95.1 ppm, also resolved in specimens *RABB* and *SBKS*. However, samples of synthetic K-feldspar of $KAlSi_3O_8$ composition, acquired either by hydrothermal crystallization from a melt at high temperature (sample *7294*) or by K→Na ion-exchange reactions at 800 °C (sample *K-EU2*) or at 1050 °C (sample *K-713r**), invariably have three maxima, approximately at the same chemical shift as found in the other K-feldspar types, as was also reported for an adularia crystal with a high-sanidine XRD pattern (Zhou et al. 2001). Note that if Na atoms are replaced with K atoms by ion exchange at 800 °C, the Si, Al distribution is not disturbed, whereas some modifications are expected in heating experiments performed at 1050 °C. No obliquity was detected in the XRD patterns of the sanidine specimens after the ion-exchange experiments. Our findings suggest the presence of more spectroscopically distinct or real-space sites than are considered by the monoclinic lattice model. It follows that the single peak at –97.0 ppm in natural sanidine must be due to the coalescence of two Si signals, T_2O (3Si,1Al) and T_2m (2Si,2Al), which is induced by the partial substitution of K atoms for the smaller Na atoms. The displacement effect is higher in the T_2m (2Si,2Al) signal, the one with a higher content of Al atoms in the second coordination sphere. The best simulations of the three-maximum sanidine spectra were obtained using: (1) the same line positions as in orthoclase and valencianite; (2) similar Si, Al occupancies as in valencianite (the t_1O value is considerably larger than the other three values); and (3) larger line widths (Fig. 4b, Table 3). Shoulders at –92.5 and particularly at –105.5 ppm are well developed in the spectrum of K-substituted sanidine, but they are not as large as in the simulated spectra.

The spectra resulting from a structure with a fully disordered Si, Al distribution, where the four sites have the same Al occupancies (i.e., $t_x = 0.25$), were also simulated either with a monoclinic structure (Fig. 4c) or a local triclinic symmetry (Fig. 4d) for sake of comparison. In the first case, only two populations of T sites are considered, i.e., –97.8 – 4.8 = –93.0 ppm for T_2O (3Si,1Al) = T_2m (3Si,1Al), whereas in the second case, the spectrum is the sum of four identical populations with different chemical shifts (triclinic high sanidine in Table 6[1]). The two simulations are farther from the experimental spectra of any sanidine specimen than the proposed model in Figure 4b, where a large t_1O value in comparison with the other three site occupancies is assumed. A decrease in the shielding at ^{29}Si between 4.0 and 5.5 ppm arising from the substitution of Al for Si atoms in the second-sphere coordination did not reproduce a profile based on two maxima only. The ^{29}Si spectrum of sanidine based on two maxima was found only in Na-rich specimens, and it is particularly far from the model of random disorder in a monoclinic lattice (Fig. 4c).

^{27}Al MAS NMR spectra

Because Loewenstein's rule was so useful in the interpretation of the ^{29}Si spectra, the Al atoms are expected to be systematically surrounded by four Si atoms, and the interpretation of the spectra could be straightforward. On this basis, one should be able to resolve signals arising from Al atoms surrounded by 4 Si at different structural sites, having different average T-O distances, by this technique. However, the second-order quadrupolar effect involves difficulties in the expected spectral resolution of the different T sites, which can be partly improved by the use of a high external magnetic field. Thus, ^{27}Al MAS NMR spectra were obtained and compared at 9.4 and 19.6 T (Table 4).

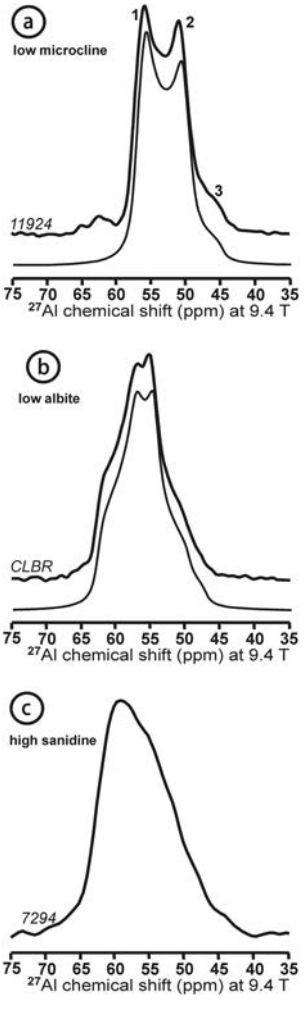

FIGURE 5. The ^{27}Al MAS NMR spectra of alkali feldspars at 9.4 T. (**a**) Specimen *11924* or untwinned K-feldspar ordered end-member (low microcline), marked with 1, 2, and 3 for the features of the quadrupolar profile of the T_1O site, simulated with δ_{iso} = 58.7 ppm, C_Q = 3.2 MHz and η = 0.2. (**b**) Specimen *CLBR* with fully ordered low albite, simulated with δ_{iso} = 62.9 ppm, C_Q = 3.17 MHz, and η = 0.65. (**c**) Sample *7294* as the disordered end-member (high sanidine) with $KAlSi_3O_8$ composition.

Figure 5 shows the central transition (C.T.) ½ → –½ in the ^{27}Al MAS NMR spectra at 9.4 T of Al atoms in tetrahedral coordination for the fully ordered end-member close to the $KAlSi_3O_8$ composition with the low-microcline XRD pattern in specimen *11924* (Fig. 5a), the $NaAlSi_3O_8$ composition with low-albite XRD pattern in specimen *CLBR* (Fig. 5b), the disordered sanidine with stoichiometric $KAlSi_3O_8$ composition in sample *7294* (Fig. 5c). The spectrum of low microcline shows a broad line due to second-order quadrupolar effects (maxima 1 and 2 and shoulder 3), ascribed to a single crystalline position of Al atoms in the T_1O site, with δ_{iso} = 58.7 ppm, C_Q = 3.2 MHz, and η = 0.2 (Kirkpatrick et al. 1985; Phillips et al. 1988; Xiao et al. 1995). The signal at around +63 ppm in Figure 5a is from a Na-feldspar impurity. Similarly, a single Al site is found in the spectrum of low albite with with δ_i = 63.1 ppm, C_Q ~ 3.2 MHz, and η = 0.65 (Kirkpatrick et al. 1985; Phillips et al. 1988). Note that the same C_Q value is used for the two simulations. However, the high-sanidine spectrum is more compatible with the presence of broad distributions of tetrahedral sites for aluminum.

Figure 6a shows the changes in the C.T. of spectra with Si, Al disorder at 9.4 T along the order-disorder series. The slightly disordered structures of intermediate microcline show the same quadrupolar lineshape structure from the T_1O site as low microcline (specimen *11924* in Fig. 5a and specimen *9544* in Fig. 6a), but it is somewhat blurred (marked with 1, 2, and 3 in specimen *116*). In this case, an additional shoulder at 61 ppm (marked as 4) is also detected. As disorder increases, the signal at 61 ppm increases, but the quadrupolar profiles cannot be recorded. In the high sanidine, a broad asymmetric signal is obtained, with a maximum between the signals 1 and 4. Figure 7 displays the variation of the first moment M_1 of the C.T., calculated between 35 and 70 ppm, vs. the line width at the middle height at this low external magnetic field. The M_1 and line width values change from 53.3 and 8.1 ppm in low microcline (specimen *11924*) to 57.1 ppm (sample *7294*) and 13.0 (specimen *EU2*) in high sanidine. This observed dispersion of data is due to variable contribution of the two components T_1 and T_2, but also to the influence of Na atoms in the solid solution as well as to Na-feldspar impurities caused by exsolution. However, it clearly shows the existence of two populations of different K-feldspars, one consisting of microcline and orthoclase, and the other, of sanidine and valencianite, which reflect different local structures. The second population shows a higher dispersion of values, but if natural *EU2* and *713r* specimens are ion-exchanged to produce pure K-feldspar as *K-EU2* and *K-713r** synthetic samples, the M_1 value is displaced from 13.0 and 12.7 to 11.7 ppm. This value is very similar to that of the synthetic *7294* sample. Such type of displacement is much smaller in ion-exchanged orthoclase (*K-ASGS*).

At 19.6 T, the C.T. signals from Al atoms are narrower than at 9.4 T (Fig. 6b) displaying again two signals from T_1 and T_2 sites. In specimen *9544*, the quadrupolar broadening at 19.6 T (marked with 1 and 2) is lower but can be simulated with comparable quadrupolar parameters as those used in specimen *11924* at 9.4 T. The increment of local disorder produces the appearance of an additional signal at the left side of the main peak, as at 9.4 T (marked with 4 for specimen *116*). The ^{27}Al spectra at 19.6 T were simulated with a quadrupolar line for the T_1 sites and a Gaussian curve for the T_2 sites, both signals becoming broader

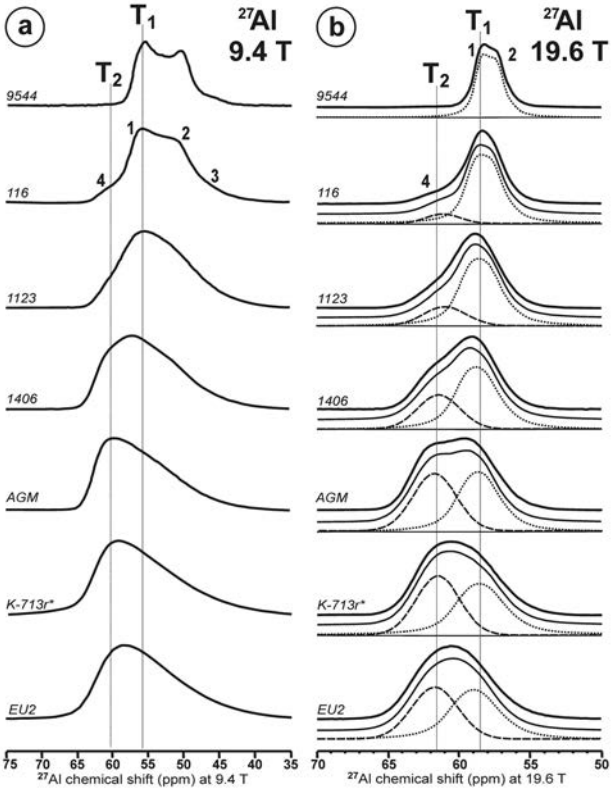

FIGURE 6. The ^{27}Al MAS NMR spectra from selected specimens and samples of (**a**) K-feldspar at 9.4 T and (**b**) 19.6 T. Signals 1, 2, and 3 can be explained as in Figure 5 from T_1 sites, and signal 4 corresponds to Al atoms in T_2 sites. Spectral simulations in **b** are performed with NMR parameters of Table 4. Dotted lines for T_1 sites and dashed lines for T_2 sites, simulated spectra as fine continuous lines, and experimental spectra as thick continuous lines.

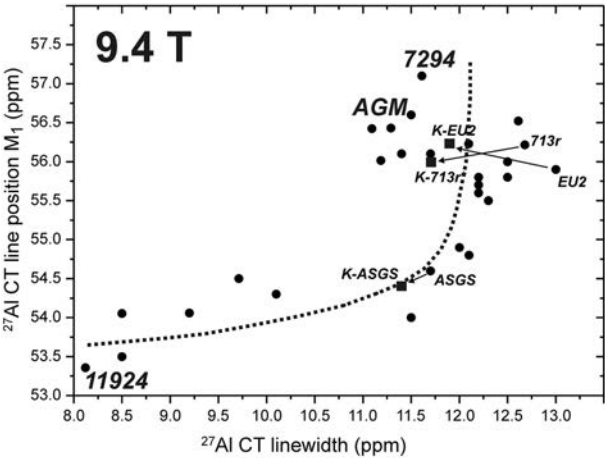

FIGURE 7. Variation of the first moment M_1 with line width in ppm from the C.T. in the ^{27}Al spectra at 9.4 T. The relationships between some natural specimens and their ion-exchanged counterpart are marked with arrows. Ordered and disordered end-members (specimen *11924* and sample *7294*) and valencianite *AGM* are also labeled.

with disorder (Table 4). The Al occupancies in these two sites were calculated from their spectral areas as Σt_1 and Σt_2 values. In the more disordered samples (natural and ion-exchanged sanidine and valencianite *AGM*), the best spectral simulations were obtained for $\Sigma t_1 > \Sigma t_2$, with a similar order-disorder parameter as that estimated from the ^{29}Si spectra. The C_Q and η parameter change from ca. 3.2 MHz and 0.25 in low microcline to 4.0 MHz and 0.5 in high sanidine, with minor but still detectable changes in the chemical shifts. Note also that disorder was simulated by increasing the line widths (i.e., the Em parameter) in the ^{27}Al spectra, as it was done also in the simulations of the ^{29}Si spectra.

The modeling of the quadrupolar parameters for the two sets of T sites is described in Figure 8, for structures close to the ordered and disordered end-members, by means of a "second-order graphic extrapolation" of the chemical shift (similar to the SORGE diagram of Massiot et al. 1995). It shows the external magnetic field dependence of the position of the centers of gravity (cg) for the C.T. of Al atoms in the two sets of T sites. The two T_1 and T_2 sites are represented by two straight lines passing through three points, the δ_{cg} at 9.4 T ($1/\nu_0^2 = 92.02 \times 10^{-4}$ MHz^{-2}), the δ_{cg} at 19.6 T ($1/\nu_0^2 = 21.06 \times 10^{-4}$ MHz^{-2}), and the intercept with the vertical axis corresponding to the δ_{iso} corrected from quadrupolar effects. For the T_1O site, the value of δ_{iso} calculated from the spectral simulation and the SORGE diagram are coincident in low microcline. However, the δ_{iso} for the T_2 sites can be inferred only from Figure 8, as this signal was simulated with Gaussian curves. Thus δ_{iso} (T_2) = 62.1 ppm was estimated for disordered Al atoms (from δ_{cg} = 61.1 ppm at 9.4 T and δ_{cg} = 61.8 ppm at 19.6 T) in intermediate microcline and orthoclase. In addition, the slope of these lines is proportional to ν_Q^2, allowing the calculation of ν_Q for the T_2 sites as ~220 kHz, less than the half of the value at the T_1O site. Similarly, the NMR parameters

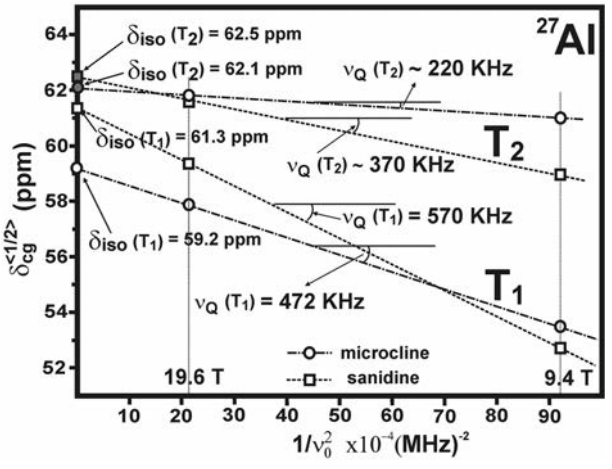

FIGURE 8. SORGE diagram for the two spectroscopically distinct sets of T sites for Al atoms for microcline and sanidine. The δ_{cg} values for the central transition are plotted with the intensity of the external magnetic field as $1/\nu_0^2$. The T_1 site in microcline from specimen *9544*, the T_2 site for intermediate microcline from specimen *116*, and T_1 and T_2 sites in sanidine from specimen *EU*2 (see explanations in the text) are here analyzed. The chemical shift values from the simulated spectra are denoted by white symbols, whereas calculated chemical shift values from this diagram are in gray.

of the T_2 site in sanidine *EU*2 were calculated as δ_{iso} = 62.5 ppm, C_Q = 2.46 MHz ($\nu_Q \approx 370$ kHz). With these values, we were finally able to simulate the C.T. at both external magnetic fields using two quadrupolar profiles if a η = 0.60 value is used for the T_2 sites (this parameter could not determined from initial simulations using Gaussian profiles).

^{39}K MAS NMR spectra

The C.T. of the ^{39}K spectrum of specimen *11924* at 19.6 T (Fig. 9a) shows a single M_1 site for the K atoms, as in the spectrum recorded by Stebbins et al. (2002) for low microcline, with δ_i = 65.2 ppm, C_Q = 1.91 MHz, and η = 0.87 (Table 4). The ^{39}K spectrum of specimen *9544* can still be fitted with a single site, but a slightly larger quadrupolar C_Q value is needed to reproduce the profile (Fig. 9a, Table 4). With increasing disorder, this quadrupolar profile becomes blurred, and at least two signals are needed for a simulation of the spectra, corresponding to two sets of spectroscopically distinct M_1 and M_2 sites inside the irregular cavity, instead of a single crystallographic M site as proposed by Taylor's model. Spectra were reproduced with a quadrupolar profile for the M_1 site and a Gaussian curve for the M_2 site, with changes in the line broadening and in asymmetry parameter η from 0.87 in low microcline to values around 0.6

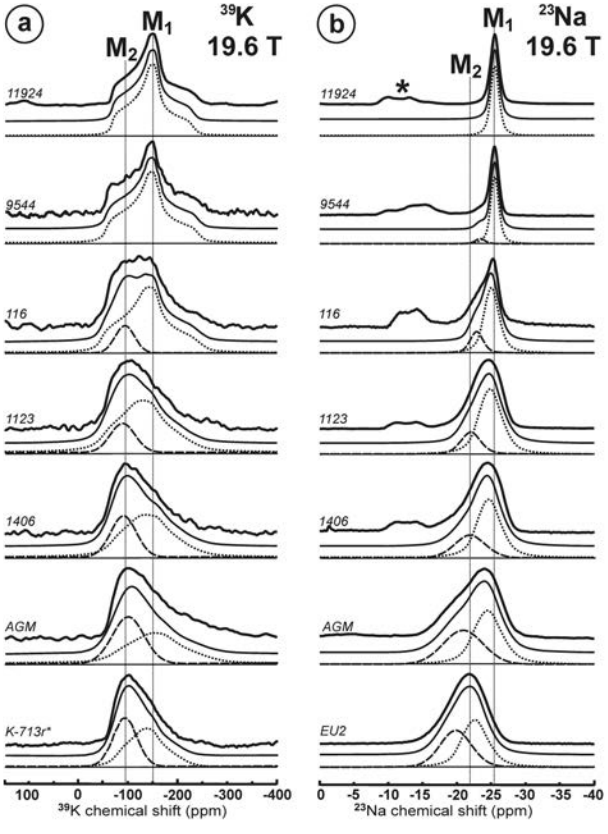

FIGURE 9. (**a**) The ^{39}K MAS NMR spectra and (**b**) ^{23}Na MAS NMR spectra of selected K-feldspars at 19.6 T. Dotted lines for M_1 sites and dashed lines for M_2 sites, simulated spectra as fine continuous lines (Table 4), experimental spectra as thick continuous lines. The asterisk "*" denotes signal from exsolved Na-rich feldspar.

in valencianite and sanidine for the M_1 site. Also, it is necessary to increase the relative intensity of the M_2 signal, without much change in their chemical shift (in comparison with estimated uncertainties). Disorder is also accompanied by an increase in the line widths (i.e., the Em parameter in spectral simulations). The site occupancies of the K atoms in these M_1 and M_2 sites were calculated from their respective areas as Σm_1 and Σm_2 values (Table 4). Figure 10 is a correlationship between the site occupancies of framework sites by Al atoms and the cavity sites by K atoms, calculated from simulated areas of the experimental spectra at 19.6 T. A linear relationship is clearly obtained along the order-disorder series.

^{23}Na MAS NMR spectra

The C.T. of the ^{23}Na spectra of selected specimens at 19.6 T are shown in Figure 9b. The NMR parameters of the simulated peak shapes are given in Table 4. The spectra of untwinned and twinned low microcline are similar at 9.4 T, but they are slightly different at 19.6 T. Spectra from specimen *11924* are compatible with a single M_1 site for Na atoms, with well-defined quadrupolar parameters, whereas an additional signal from the M_2 site is detected in specimen *9544*. This signal from the M_2 site does not overlap with a broad signal from the Na atoms of Na-feldspar in exsolution lamellae and impurities (marked with an asterisk in specimen *11924*, Fig. 9). Na-feldspar is absent in sanidine *EU*2 and valencianite *AGM* as shown in spectra of Figure 9b. Again, all the spectra were simulated with a quadrupolar profile for the M_1 site and a Gaussian curve for the M_2 site. With disorder in the Si, Al distribution, the relative area of the signal from Na atoms in the M_2 site increases, displaying similar Na occupancies in the two sites in spectra obtained at 9.4 and 19.6 T. In general terms, the simulation of the ^{23}Na spectra is also consistent with that of ^{39}K spectra, giving comparable Σm_1 and Σm_2 occupancies. The relationship between the occupancies of framework sites by Al atoms and cavity sites by Na atoms is parallel to that represented in Figure 10. In other words, no clear segregation of alkali atoms in these sites was noted. However, a sharp increase in the C_Q for the M_1 site, a line width increase for the M_2 site, and some peak shifts were noted with progressive disorder, effects that were investigated in detail with the help of the SORGE diagram (Fig. 11). The values of the NMR parameters for the M_1 site from this diagram are also well matched with those quantities estimated from individual simulations. However, for the M_2 site, the C_Q and δ_{iso} parameters can only be estimated from the SORGE diagram, using the δ_{cg} values measured from the Gaussian profiles of the spectral simulations to calculate the ordinate for $x = 0$ and the line slopes. In this way, δ_{iso} at –20.3 and –18.7 ppm and C_Q of 1.07 and 1.46 MHz were obtained for the M_2 sites in low microcline and high sanidine, respectively. Using these values, the quadrupolar profiles for the M_2 site were reasonably reproduced for $\eta \approx 0.70$ in the original spectra at both external magnetic fields.

Discussion

Local structures in K-feldspar

Structural states in K-feldspar are conventionally defined between two end-members or stable thermodynamic phases: low microcline for the fully ordered end-member and high sanidine for the totally disordered end-member. These states are described with very specific lattice models from reciprocal-space techniques. Orthoclase is generally considered to be an intermediate and metastable state, whereas valencianite is described as an unstable phase (Smith 1974).

Figure 12a exhibits the triclinic $C\bar{1}$ model of low microcline, in which the four T sites have a fixed Al occupancy defined as $t_1O = 1.0$ and $t_1m = t_2O = t_2m = 0.00$, and a single M site for K atoms. Two structural layers are schematically represented, with four four-membered rings of tetrahedra, labeled 1 to 4, in two

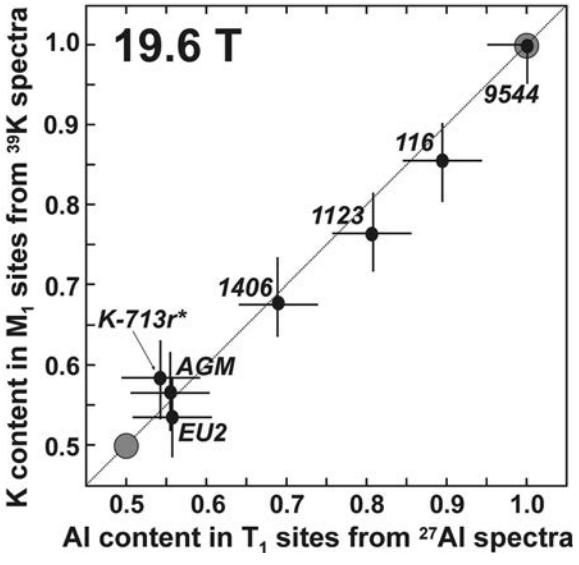

Figure 10. Correlationship between Σt_1 from Al atoms in T_1 sites and Σm_1 from K atoms in M_1 sites from spectral simulations (Table 4) of experimental spectra at 19.6 T.

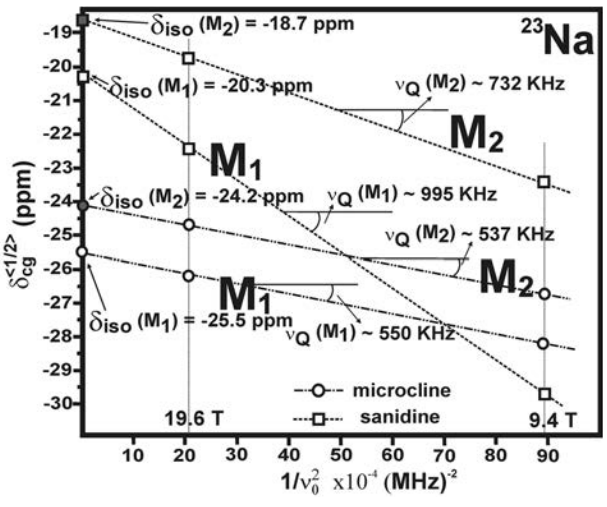

Figure 11. SORGE diagram for the two spectroscopically distinct sets of M sites for Na atoms, where the δ_{cg} values for the C.T. are plotted with the external magnetic field as $1/\nu_0^2$. M_1 and M_2 sites from twinned low microcline (specimen *9544*) and high sanidine (specimen *EU*2) with symbols as in Figure 8 (see explanations in the text).

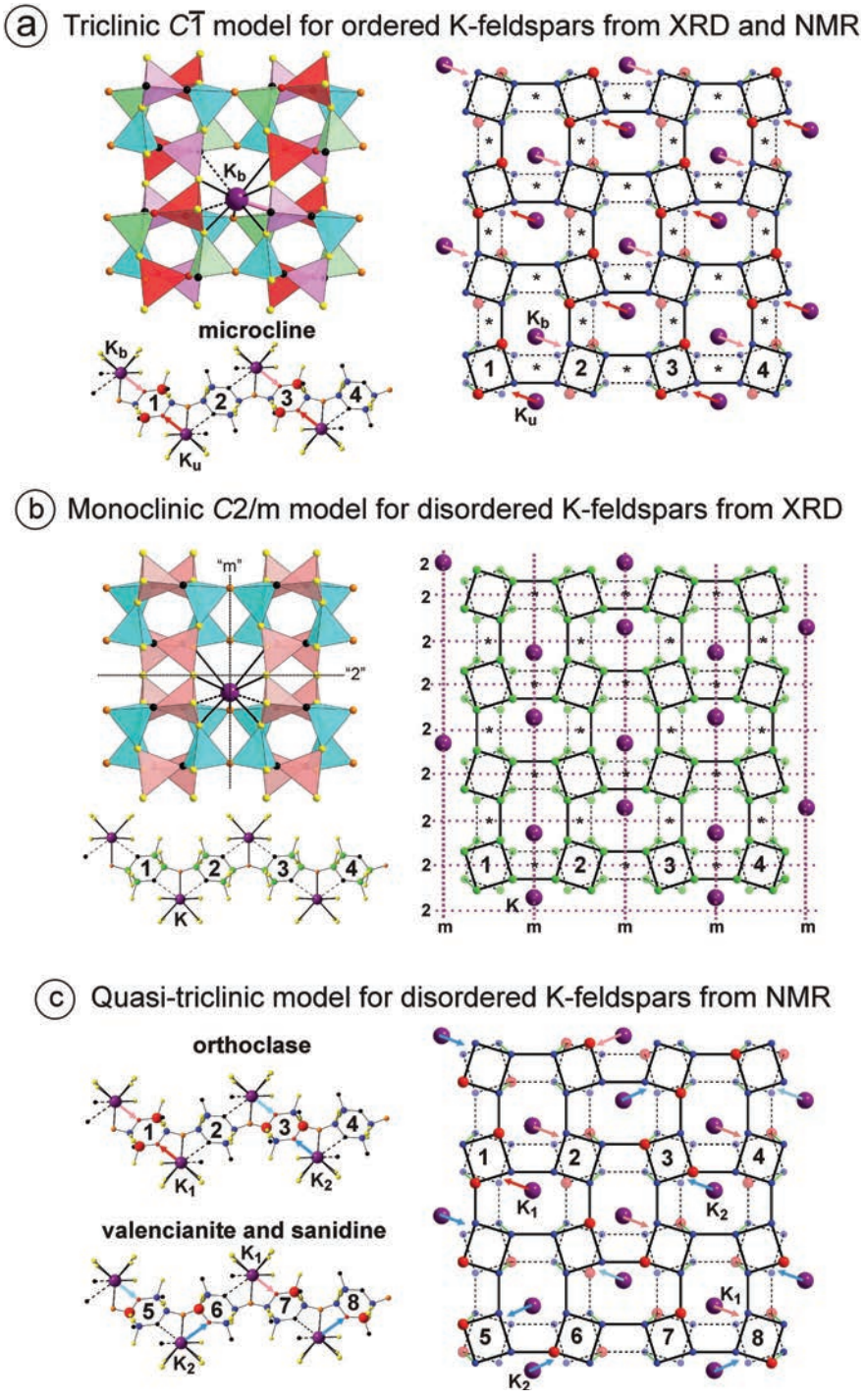

FIGURE 12. Lattice models of low microcline (**a**) and high sanidine (**b**) from XRD; "m" mirror plane, "2" twofold binary axis, and "*" inversion centers. (**c**) Quasi-triclinic model with MRO from NMR for orthoclase, valencianite, and sanidine. The projection normal to the *a* axis show two sheets of T sites with the interlayer M sites, and onto the (001) plane display a chain of T atoms along the *b* axis and related K atoms at different height. The K-O_{CO} bonds (absent in the monoclinic model) are in dark red for K_u (up) and light red for K_d (down). Four 4-membered rings of T sites are marked with numbers in the two projections. The T_1 sites are in pink and T_2 sites in blue for the *C*2/*m* model in **b**, whereas T_1O sites in red, T_1m sites in purple, T_2O sites in blue, and T_2m sites in green for the *C*$\bar{1}$ model in **a**; green color for both Si and Al atoms in **b**, and blue for Si atoms and red for Al atoms in **a**; the O_{A1} oxygen atoms are in orange, the other oxygen atoms are in yellow; oxygen atoms not bonded to K (at larger distances than 3.12 Å) are in black and with discontinuous lines. In **c**, the rings 1 to 4 correspond with orthoclase, and rings 5 to 8 with valencianite and sanidine, M_1 sites with red arrows, M_2 with blue arrows. Structural data: Blasi et al. (1984a) for microcline; Kimata et al. (1996a) for sanidine (see text for details). (Color online.)

complementary orientations (bottom left and right schemes, Fig. 12a). The ring structures have perfect alternation in the number of Al atoms (in red color) per ring, shown as "…-2-0-2-0-…" chains along the b axis (as well as perpendicularly) in the upper layer and "…-0-2-0-2-…" in the lower layer. A coordination of the K atom by seven oxygen atoms emerges for K-O distances less than ~3.02 Å (Downs et al. 1996). Two K-O_{CO} bonds exist here in each four-T ring with two Al atoms (one in dark red related to the K_u atom if this bond points up, the other in light red at the K_d atoms when it points down, O_{CO} atoms in red color). The K-O_{Cm} distances are greater than 3.12 Å (discontinuous lines and oxygen atoms in black color), and thus O_{Cm} atoms are underbonded with K atoms. The NMR data of the untwinned low microcline (specimen *11924* with $t_1O = \Sigma m_1 = 1.0$ and $t_2m \approx t_2o \approx t_1m \approx \Sigma m_2 = 0.00$) are entirely consistent with that model to produce perfect long-range periodicity. The non-equivalent crystallographic sites, defined with invariant atomic coordinates from the average structure after Bragg diffractions, are equivalent to spectroscopically distinct sites in the form of specific local chemical environments with fixed quadrupolar parameters and chemical shifts from NMR spectra.

Figure 12b shows two structural layers of tetrahedra of the monoclinic *C*2/*m* model of high sanidine ($t_1O = t_1m = t_2O = t_2m = 0.25$), in which the mirror plane "m", twofold "2" axes, and inversion centers are schematically represented. The rings do not show the Si and Al occupancies (i.e., the two shown in green) and the cavity atoms rest in a single M site located at the mirror plane, for a random distribution of the framework cations. In other words, the ionicity of the K atoms and the monoclinic symmetry for the topology of tetrahedra were formally linked in Taylor's original model to describe structural disorder. The K-O_C distances are larger than 3.12 Å, and thus, O_C atoms (in black) are underbonded (discontinuous lines) by the K atoms, although a coordination with seven oxygen atoms exists from K-O distances lower than ~3.02 Å (as it was used for microcline in Fig. 12a). Substitutional disorder in the framework could be associated with positional disorder inside the cavity.

Our data support structural features and constraints not fully recognized in this conventional model for disorder, as follows. Two T sites and a single M site were not detected by NMR experiments. The ^{29}Si spectra at 9.4 T and the ^{27}Al spectra at 19.6 T have shown in all cases $\Sigma t_1 > \Sigma t_2$ if the Al occupancies are inferred from the relative areas of peaks. The chemical shifts of the T_1 and T_2 sites in the ^{29}Si and ^{27}Al spectra are equivalent when the same chemical environment is compared, i.e., $(\delta T_1O + \delta T_1m)/2 < (\delta T_2O + \delta T_2m)/2$ for Si atoms, and $\delta_{iso}T_1 < \delta_{iso}T_2$ for Al atoms. The lower C_Q value for Al atoms in T_2 sites (Fig. 8c) could indicate that this site is locally less distorted than the T_1 site. The η parameter for the T_1 sites decreases slightly from sanidine to microcline, indicating lower distortions in these sites with increasing disorder. Thus the T_1 and T_2 sites are very different from the spectroscopic point of view. All of these data unequivocally indicate that random disorder of the framework cations must be very uncommon or nonexistent. Positional disorder involves slightly variable bond-distances and bond-angles, which cause distributions of isotropic chemical shifts and quadrupolar parameters produced by electric field gradients (EFG), as we also noted in the NMR spectra of the alkali cations.

The simulations of the ^{29}Si spectra can be used to calculate a mean local obliquity Δ from the chemical shifts of the different sites with the same chemical environment; for instance, for T_x ($3Si,1Al$) we can define Δ as $[(\delta T_1O - \delta T_1m) + (\delta T_2O - \delta T_2m)]/2$. We have found that in intermediate microcline close to the low microcline (specimen *176*) Δ is 1.85 ppm; in orthoclase Δ is 1.5 ppm, and in sanidine and valencianite Δ is 1.35 ppm. A Δ value of 0.0 must occur for strictly monoclinic symmetry where $\delta T_1O = \delta T_1m$ and $\delta T_2O = \delta T_2m$ (as in models shown in Figs. 2c and 4c), but this was not observed in any of the experimental spectra. This finding implies that analogous triclinic-like distortions exist for all structures along the order-disorder series at room temperature, with four spectroscopically distinct T sites having $t_1O \neq t_1m$, $t_2O \neq t_2m$, instead of two T sites for sanidine and four T sites for microcline.

The ^{39}K and ^{23}Na spectra demonstrate the existence of a single M site for alkali atoms only in untwinned low microcline close to the stoichiometric $KAlSi_3O_8$ composition, which is extremely rare in nature. Two sets of M site distributions can be resolved if some disorder exists in the framework of tetrahedra. The C_Q parameter for the M_1 site derived from the ^{39}K spectra do not change significantly along the order-disorder series, whereas the same parameter for the T_1 site from the ^{27}Al spectra clearly increases. It could indicate similar local environments for K atoms but growing tetrahedral distortions when disorder increases. Thus, the local geometry of the framework cations seems to be forced to change to accommodate framework disorder, whereas the local geometry in the M_1 site for K atoms is better preserved. The same adaptive behavior to disorder is found for Na atoms as the C_Q values from the ^{23}Na spectra increase progressively from low microcline to high sanidine. In addition, the SORGE diagrams indicate $C_Q(T_1) > C_Q(T_2)$ from ^{27}Al spectra as $C_Q(M_1) > C_Q(M_2)$ from ^{23}Na spectra, with similar η parameter in all cases. Note also that δ_{iso} for Na atoms in M_1 sites is lower than in M_2 sites, as can also be inferred for the K atoms. Hence, the NMR data show a remarkable internal consistency if data from the different nuclides are compared. In addition, no segregation of alkali atoms in the M sites is noted.

Structural models featuring an alkali site split into two half-occupied or four quarter-occupied sites have been proposed for disordered Na-feldspar (Ribbe et al. 1969; Prewitt et al. 1976; Winter et al. 1979), hypersolvus alkali feldspars (Fenn and Brown 1977; Salje 1986), disordered Li-feldspar (Baur et al. 1996), as well as in plagioclase (Fitz Gerald et al. 1986) on the basis of the highly anisotropic shape of the electron-density distribution surrounding alkali atoms in single-crystal XRD refinements. Because of the domain structure in some of these disordered feldspars and the limited resolution of diffractometric techniques, non-equivalent positions for alkali atoms are difficult to distinguish from spatial average effects due to slightly disoriented domains. As a result, it is hard to distinguish site distributions from positional disorder of discrete structural sites with XRD techniques. Because the NMR measurements are not averaged over domains or twin microstructures at the mesoscale, which are totally absent in valencianite and sanidine, we can conclude that split sites for alkali atoms must be considered also in disordered K-feldspars.

If we correlate the site occupancy of framework and cavity

cations on the basis of ^{27}Al, ^{39}K, and ^{23}Na spectra at 19.6 T, a linear relationship is outlined along the entire order-disorder series (Fig. 10). In addition, the increase in the C_Q values for Al atoms at the T_1 and T_2 sites with framework disorder is also correlated with the same trend for the Na atoms in the M_1 and M_2 sites, indicating the increment of disorder. The departure from overall monoclinic symmetry at a local scale thus is connected with multi-site correlations or chemical coupling between Al atoms and alkali atoms to form molecular-like Al(T_2)-O-K(M_2) and Al(T_1)-O-K(M_1) linkages. Hence, "real" M sites with energy minima inside a single type of irregular cavity for the alkali atoms are formed as requirements of the Si, Al distribution, as a consequence of local charge-balancing mechanism at the atomic scale. On this basis, a general model for disordered structures can be proposed with a quasi-triclinic local symmetry (i.e., the twofold axis, the mirror plane and the inversion centers are absent at the medium-range scale) as in Figure 12c. The Al atoms (in red) are distributed over different four-T rings related to O_{CO} or O_{Cm} oxygen atoms (also in red), which are bonded with K atoms. Where Al atoms are at T_1 sites, K_1-O are formed (red arrows), where Al atoms are at T_2 sites K_2-O bonds exist (blue arrows), with overall maintenance of the seven coordination of K by oxygen atoms.

Medium-range order in disordered K-feldspar

The crystal structures of long-range disordered K-feldspars can be described by the ring structures over medium-range length scale, with structural correlations in the range of 0.5–2.0 nm according to the number of Al atoms per each four-T ring, which is closely associated with the disposition of the alkali atoms. The medium-range order (MRO) of K-feldspar explains their diversity in two broad groups, microcline and orthoclase on the one hand, and valencianite and sanidine on the other hand.

Microcline. Some disorder is detected only in the ^{23}Na spectrum in regularly twinned low microcline (specimen 9544). It may be associated with structural distortion at Na-rich broad twin boundaries (Sánchez-Muñoz et al. 1998, 2006b). Intermediate microcline has a more disordered structure, and the simulations of the ^{29}Si spectra are consistent with $t_1O >> t_2m > t_2O \approx t_1m$ values. Interestingly, a high-t_1O value seems to be associated with a very low t_1m value (a characteristic that is developed more clearly in orthoclase), but a structure of "…-2-0-2-0-…" chains with "Al(T_1O)-Si(T_2m)-Al(T_1O)-Si(T_2m)" rings must be a major feature.

This framework arrangement does not follow Dempsey's rule that, based on electrostatic arguments, suggests the number of Al-O-Si-O-Al linkages tend to a minimum (i.e., the Al atoms assume the largest possible separation) for a given Si/Al ratio value (Dempsey et al. 1969). Thus, the microcline structures could be analogous to that of hydrogen faujasite where two Si atoms and two Al atoms also form four-membered rings with Si-O-Al bridges at opposite sides, with local stabilization by bonded protons at the bridging oxygen atoms (Schröder and Sauer 1993).

Orthoclase. The ^{29}Si spectra are consistent with $t_1O > t_2m > t_2O \approx t_1m$ with $t_1O + t_2m \approx 0.9$, i.e., our findings imply that Al atoms are preferentially located at T_1O-T_2m-T_1O-T_2m rings. A relatively high Al content at the T_2m site has not been suggested from XRD methods in orthoclase, as only T_1 and T_2 sites are distinguished in the structural lattice model with monoclinic symmetry. However, mean T_2m-O distances larger than the T_2O-O and T_1m-O distances do exist in high albite (Taylor 1965). It is not possible to discriminate between different Al occupancies of the T sites and intrinsic structural differences in these sites on the basis of X-ray data only (Winter et al. 1979). Because of Loewenstein's rule of Al-O-Al avoidance, Al atoms cannot occupy T_1O and T_1m sites in the same four-T ring, and consequently two types of rings with "…-2-0-2-0-…" arrangements must alternate along the chains of tetrahedra as "Al(T_1O)-Si(T_2m)-Al(T_1O)-Si(T_2m)" (rings 1 to 4 in Fig. 12a) and "Si(T_1O)-Al(T_2m)-Si(T_1O)-Al(T_2m)" (rings 1 to 4 in Fig. 12c).

The natural abundance and persistence of orthoclase in igneous, metamorphic, and hydrothermally affected rocks, have been interpreted as resulting from a small driving force for ordering once structural modulations are formed, involving the formation and coexistence of ordered and anti-ordered domains (Eggleton and Buseck 1980) and a domain-texture barrier effect (Brown and Parsons 1989). However, it is difficult to imagine extended ordering processes at the subsolidus stage in K-feldspar of hydrothermal origin, because of the low temperature of crystallization. In this case, the observable state of order must be very close to that originally formed during growth. One can envision that it will be very difficult to reverse configuration of atoms where the Al occupancy forms that type of four-T rings, because the ordering reactions cannot occur by a single atomic jump, as an Al atom at the T_2m site avoids the location of another Al atom at the T_1O site in the same four-T ring. Therefore, this particular medium-range order scheme (orthoclase in Fig. 12c) can explain the metastability, attainability, and preservation of orthoclase, in spite of the presence of H_2O in the environment.

Valencianite. The ^{29}Si spectra in this type of K-feldspar are compatible with $t_1O > t_2O > t_1m \approx t_2m$ values in the less strongly disordered samples and $t_1O > t_2O \approx t_1m \approx t_2m$ values in the more strongly disordered ones. However, the (3Si,1Al) and (2Si,2Al) environments seem to be much more abundant than in a simple model obeying Loewenstein's rule. Therefore, the most characteristic feature of valencianite is the expression of some Si, Al order (involving strong deficiency of Si atoms in Q^4 (4Si,0Al), (1Si,3Al), and (0Si,4Al) environments) not accounted for in a conventional disorder model, which assumes purely random distribution of Si and Al neighbors once Loewenstein's rule is respected. This particular order, in such low-temperature structures, is compatible with a medium-range scale configuration in which mainly only one Al atom occurs per four-T rings to give "…-1-1-1-1-…" chains as in rings 5 to 8 in Figure 12c.

Sanidine. The ^{29}Si spectra of natural specimens and synthetic samples are also compatible with $t_1O \neq t_1m$ and $t_2O \neq t_2m$, with a t_1O value higher than the Al occupancy of the other three sites, involving triclinic-like local distortions as noted from the chemical shifts. Loewenstein's rule of Al-O-Al avoidance seems to be respected, as in other framework aluminosilicates (Klinowski et al. 1982; Phillips and Kirkpatrick 1995). However, the (4Si,0Al) and (0Si,4Al) environments are less developed in experimental than in the simulated spectra, which are closer to experimental ones than in the case of valencianite. Hence, the "…-1-1-1-1-…" chain configuration could be still valid for this high-temperature structure, although the additional effect of dispersion of charges

seems to be less well developed than in valencianite. In our interpretation, sanidine forms directly as a quasi-triclinic modification, or it undergoes displacive-like transformations on cooling, or both. Extensive Si, Al ordering on cooling cannot be invoked in unexsolved natural Na-rich specimens and in samples obtained via ion-exchange experiments.

IMPLICATIONS

Two complementary implications are derived from previous experimental data and discussion, one at the level of K-feldspar systematics and nomenclature, the other related to the understanding of the K-feldspar crystalline solid-state.

The IMA only recognizes three terms for K-feldspar mineral species, namely sanidine, orthoclase, and microcline (Barth 1934). However, "valencianite" can be described with a crystal structure having not only the distinctive characteristics of triclinicity and disorder, but also a particular MRO atomic scheme, as suggested from the NMR data of this work. Thus, perhaps "valencianite" can be considered also as a mineral species of the K-feldspar group. This K-feldspar is likely to be of high interest in the study of authigenic rocks and mineral deposits from epithermal environment.

Solids are commonly seen from a sharp twofold perspective, either as crystalline or non-crystalline, having (or not) atomic order on a scale that produces an indexable diffraction pattern (IUCr 1992; Nickel 1995). In crystalline solids, short-range order (SRO) arises from atomic forces resulting in the first sphere of coordination, whereas long-range order (LRO) is the consequence of periodicity (Lifshitz 2007). Where crystals have perfect LRO (i.e., the distances of atomic correlations are much longer than the size of coherent diffraction), reciprocal-space techniques are able to resolve structural arrangements at the atomic scale as lattice models in "ideal" crystal structures.

However, the discovery of quasicrystals involves the unequivocal existence of solids with LRO without periodicity, and leads to the modern debate of *what is a "crystal"* (Desiraju 2003; Lifshitz 2007). In addition, it is worth considering to what extent the concept of space group needs to be amended in disordered structures (Welberry 2004). Disordered, modulated, and incommensurated crystals have strictly non-periodic structures and site distributions, but their "real" structure can in principle be described with a periodic "ideal" average from the analysis of the concentrated intensity at Bragg peaks (i.e., ignoring diffuse scattering).

Feldspars (the most abundant minerals in the crust of the Earth and Moon) are particularly relevant in this debate because: (1) disorder was expressed in terms of a periodic average structure for the first time in sanidine by XRD (Taylor 1933); (2) the modulated and incommensurated structures of feldspars are currently described using the concept of an average structure (Taylor 1965; Ribbe 1984, 1994), and (3) diffuse scattering is ubiquitous (Laves 1950; Gay 1953; Jagodzinski 1984; Pleger 1996). We have shown in the present study that the NMR data cannot be interpreted with available lattice models where long-range disorder exists. *Major* substitutional Si, Al disorder in T sites is not coupled only with *minor* positional disorder for K atoms inside the irregular cavity in a K-feldspar. Non-equivalent atoms and site distributions due to positional disorder are both superposed at the same lattice site in the overlapped image offered by XRD, owing to a lack of intrinsic spatial resolving power. More importantly, the average-structure approach in strictly non-periodic disordered crystals fails to recognize essential chemical medium-range order (MRO). This means that "real" structural features at the local scale can be hidden if "ideal" long-range periodicity is imposed. Obviously, the lattice model is unsuccessful in describing crystallinity based on MRO schemes that do not form extended periodic arrangements.

ACKNOWLEDGMENTS

This work was partially supported by the National High Magnetic Field Laboratory through National Science Foundation Cooperative Agreement (DMR-0084173) and by the State of Florida. L.S.M. thanks projects MAT2010-21088-C03-01 and MAT2010-17753 for additional financial support. We thank Francois Delbove for sample *7294*, Ray Berry for specimen *11924*, and Museo Geo-Minero (IGME) in Madrid, Museo Nacional de Ciencias Naturales (MNCN, CSIC) of Madrid, and Museé d'Histoire Naturelle de Paris, for the K-feldspar specimens used in this work. We also thank to Olivier Rouer (ISTO, CNRS, France) for the results of the EMPA chemical analyses. In addition, we thank Robert F. Martin and two anonymous reviewers for the suggestions and constructive comments, as well as associate editor Brian Phillips for their help in improving this work.

REFERENCES CITED

Anbalagan, G., Sankari, G., Ponnusamy, S., Thilak Kumar, R., and Gunasekaran, S. (2009) Investigation of silicate mineral sanidine by vibrational and NMR spectroscopic methods. Spectrochimica Acta Part A: Molecular and Biomolecular Spectroscopy, 74, 404–409.

Akizuki, M., and Sunagawa, I. (1978) Study of sector structure in adularia by means of optical microscopy, infra-red absorption, and electron microscopy. Mineralogical Magazine, 42, 453–462.

Bambauer, H.U., Krause, C., and Kroll, H. (1989) TEM investigation of the sanidine/microcline transition across metamorphic zones: the K feldspar varieties. European Journal of Mineralogy, 1, 47–58.

Barth, T.F.W. (1934) Polymorphic phenomena and crystal structure. American Journal of Science, 227, 273–286.

Baur, W.H., Joswig, W., and Müller, G. (1996) Mechanics of the feldspar framework; crystal structure of Li-feldspar. Journal of the Solid State Chemistry, 121, 12–23.

Blasi, A. (1984) The variation of the 2θ angles in powder diffraction patterns of one- and two-step K-rich feldspars. Bulletin de Minéralogie, 107, 437–445.

Blasi, A., Brajkovic, A., De Pol Blasi, C., Foord, E.E., Martin, R.F., and Zanazzi, P.F. (1984a) Structure refinement and genetics aspects of a microcline overgrowth on amazonite from Pikes Peak batholiths, Colorado, U.S.A. Bulletin de Minéralogie, 107, 411–422.

Blasi, A., Brajkovic, A., and De Pol Blasi, C. (1984b) Dry-heating conversion of low microcline to high sanidine via a one-step disordering process. Bulletin de Minéralogie, 107, 423–435.

Brown, W.L., and Parsons, I. (1989) Alkali feldspars: ordering rates, phase transformation and behavior diagrams for igneous rocks. Mineralogical Magazine, 53, 25–42.

Brown, G.E., Hamilton, W.C., Prewitt, C.T., and Sueno, S. (1974) Neutron diffraction study of Al/Si ordering in sanidine: a comparison with X-ray diffraction data. In WS. MacKenzie and J. Zussman, Eds., Feldspars, p. 68–80. Manchester University Press, U.K.

Chaison, U. (1950) The optics of triclinic adularia. Journal of Geology, 58, 537–547.

Dempsey, E., Kuhl, G.H., and Olson, D.H. (1969) Variation of the lattice parameter with aluminum content in synthetic sodium faujasites. Evidence for ordering of the framework ions. Journal of Physical Chemistry, 73, 387–390.

Desiraju, G.R. (2003) In search of clarity. Nature, 423, 485.

Downs, R.T., Andalman, A., and Hudacsko, M. (1996) The coordination number of Na and K atoms in low albite and microcline as determined from a procrystal electron-density distribution. American Mineralogist, 81, 1344–1349.

Eggleton, R.A., and Buseck, P.R. (1980) The orthoclase-microcline inversion: a high resolution transmission electron microscope study and strain analysis. Contributions to Mineralogy and Petrology, 74, 123–133.

Fenn, P.H., and Brown, G.E. (1977) Crystal structure of a synthetic, compositionally intermediate, hypersolvus alkali feldspar: evidence for Na, K site ordering. Zeitschrift für Kristallographie, 145, 124–145.

Fitz Gerald, J.D., Parise, J.B., and Mackinnon, I.D.R. (1986) Average structure of an An_{48} plagioclase from the Hogarth Ranges. American Mineralogist, 71, 1399–1408.

Gay, P. (1953) The structures of the plagioclase feldspars: III. An X-ray study of anorthites and bytownites, Mineralogical Magazine, 30, 169–177.

IUCr (1992) International Union of Crystallography: Report of the executive

committee for 1991. Acta Crystallographica, A48, 928.
Jagodzinski, H. (1984) Determination of modulated structures. Bulletin de Minéralogie, 107, 455–466.
Keefer, K.D., and Brown, G.E. (1978) Crystal structures and composition of sanidine and high albite in cryptoperthitic intergrowth. American Mineralogist, 63, 1264–1273.
Kimata, M., Saito, S., Shimizu, M., Iida, I., and Matsui, T. (1996a) Low-temperature crystal structure of orthoclase and sanidine. Neues Jahrbuch für Mineralogie Abhandlungen, 171, 199–213.
Kimata, M., Shimizu, M., and Saito, S. (1996b) High-temperature crystal structure of sanidine. The crystal structure of sanidine at 935°C. European Journal of Mineralogy, 8, 15–24.
Kirkpatrick, R.J., Kinsey, R.A., Smith, K.A., Henderson, D.M., and Oldfield, E. (1985) High resolution solid-state sodium-23, aluminum-27, and silicon-29 nuclear magnetic resonance spectroscopic reconnaissance of alkali and plagioclase feldspars. American Mineralogist, 70, 106–123.
Klinowski, J., Ramdas, S., Thomas, J.M., Fyfe, C.A., and Hartman, J.S. (1982) A re-examination of Si, Al ordering in zeolites NaX and NaY. Journal of the Chemical Society, Faraday Transactions 2: Molecular and Chemical Physics, 78, 1025–1050.
Kroll, H., and Ribbe, P.H. (1987) Determining (Al,Si) distribution and strain in alkali feldspars using lattice parameters and diffraction peak positions: a review. American Mineralogist, 72, 491–506.
Kroll, H., Schmiemann, I., and von Cölln, G. (1986) Feldspar solid solutions. American Mineralogist, 71, 1–16.
Laves, F. (1950) The lattice and twinning of microcline and other potash feldspars. Journal of Geology, 58, 548–571.
Laves, F., and Goldsmith, J.R. (1961) Polymorphism, order, disorder, diffusion and confusion in the feldspars. Cursillos y Conferencias, 8, 71–80.
Laves, F., and Hafner, F. (1962) Infrared absortion effects, nuclear magnatic resonance and structure of feldspars. Norsk Geologisk Tidsskrift, 42, 57–72.
Le Bail, A., Duroy, H., and Fourquet, J.L. (1988) Ab-initio structure determination of $LiSbWO_6$ by X-ray powder diffraction. Materials Research Bulletin, 23, 447–452.
Lifshitz, R. (2007) What is a crystal? Zeitschrift für Kristallographie, 222, 313–317.
Lippmaa, E., Mägi, M., Samoson, A., Engelhardt, G., and Grimmer, A.-R. (1980) Structural studies of silicates by solid-state high-resolution ^{29}Si NMR. Journal of the American Chemical Society, 102, 4889–4893.
Loewenstein, W. (1954) The distribution of aluminum in the tetrahedra of silicates and aluminates. American Mineralogist, 39, 92–96.
Massiot, D., Müller, D., Hübert, T., Schneider, M., Kengens, A.P.M., Coté, B., Coutures, J.P., and Gessner, W. (1995) Double rotation and magic-angle spinning nuclear magnetic resonance study of ^{27}Al: reexamination of the aluminum borate $9Al_2O_3{\cdot}2B_2O_3$. Solid State Nuclear Magnetic Resonance, 5, 175–180.
Massiot, D., Fayon, F., Capron, M., King, I., Le Calvé, S., Alonso, B., Durand, J.O., Bujoli, B., Gan, Z.H., and Hoatson, G. (2002) Modelling one and two-dimensional solid-state NMR spectra. Magnetic Resonance in Chemistry, 40, 70–76.
McConnell, J.D.C. (1965) Electron optical study of effects associated with partial inversion in a silicate phase. Philosophical Magazine, 11, 1289–1301.
McLaren, A.C., and Fitz Gerald, J.D. (1987) CBED and ALCHEMI investigation of local symmetry and Si/Al ordering in K-feldspars. Physics and Chemistry of Minerals, 14, 281–292.
Megaw, H.D. (1956) Notation for feldspar structures. Acta Crystallographica, 9, 56–60.
——— (1959) Order and disorder in the feldspars, I. Mineralogical Magazine, 32, 226–241.
Nickel, E.H. (1995) The definition of a mineral. The Canadian Mineralogist, 33, 689–690.
O'Brient, J.D. (1986) Preservation of primary magmatic features in subvolcanic pegmatites, aplites and granite from Rabb Park, New Mexico. American Mineralogist, 71, 608–624.
Phillips, B.L., and Kirkpatrick, R.J. (1995) High-temperature ^{29}Si MAS NMR spectroscopy of anorthite ($CaAl_2Si_2O_8$) and its $P\bar{1}$–$I\bar{1}$ structural phase transition. Physics and Chemistry of Minerals, 22, 268–276.
Phillips, B.L., Kirkpatrick, J., and Hovis, G.L. (1988) ^{27}Al, ^{29}Si and ^{23}Na MAS NMR study of an Al, Si ordered alkali feldspar solid solution series. Physics and Chemistry of Minerals, 16, 262–275.
Pleger, S. (1996) Diffuse X-ray scattering of homogeneous potassium-rich low- and high-temperature sanidines. Zeitschrift für Kristallographie, 211, 293–298.
Prewitt, C.T., Sueno, S., and Papike, J.J. (1976) The crystal structures of high albite and monalbite at high temperatures. American Mineralogist, 61, 1213–1225.
Ribbe, P.H. (1983) Chemistry, structure and nomenclature of feldspars. In P.H. Ribbe, Feldspar Mineralogy, vol. 2, p. 1–19. Reviews in Mineralogy, Mineralogical Society of America, Chantilly, Virginia.
——— (1984) Average structures of alkali and plagioclase feldspars: systematic and applications. In W.L. Brown, Ed., Feldspars and Feldspathoids, p. 1–54. NATO C137, D. Reidel Publishing Company, Dordrecht.
——— (1994) The crystal structures of the aluminium-silicate feldspars. In I. Parsons, Ed., Feldspars and Their Reactions, p. 1–49. NATO C421, Dordrecht.
Ribbe, P.H., Megaw, H.D., Taylor, W.H., Ferguson, R.B., and Traill, R.J. (1969) The albite structures. Acta Crystallographica, B25, 1503–1518.
Rodriguez-Carvajal, J. (1993) Recent advances in magnetic-structure determination by neutron powder diffraction. Physica B, 192, 55–69.
——— (2001) Reference Guide, V. 1.9c. Laboratoire Léon-Brillouin, CEA-CNRS, France.
Roisnel, T., and Rodriguez-Carvajal, J. (2001) WinPLOTR: A Windows tool for powder diffraction pattern analysis. In Delhez, R., and Mittemeijer, E.J., Eds., Materials Science Forum, vol. 378–381, p. 118–123. Scientific.net.
Salje, E. (1986) Raman spectroscopic investigation of the order parameter behavior in hypersolvus alkali feldspars: displacive phase transitions and evidence for Na-K site ordering. Physics and Chemistry of Minerals, 13, 340–346.
Sánchez-Muñoz, L., Nistor, L., Van Tendeloo, G., and Sanz, J. (1998) Modulated structures in $KAlSi_3O_8$: a study by high resolution electron microscopy and ^{29}Si MAS-NMR spectroscopy. Journal of Electron Microscopy, 47, 17–28.
Sánchez-Muñoz, L., García-Guinea, J., Sanz, J., Correcher, V., and Delgado, A. (2006a) Ultraviolet luminescence from defects complexes in the twin boundaries of K-feldspar. Chemistry of Materials, 18, 3336–3342.
Sánchez-Muñoz, L., Correcher, V., Turrero, M.J., Cremades, A., and García-Guinea, J. (2006b) Visualization of elastic strain fields by the spatial distribution of the blue luminescence in a twinned microcline crystal. Physics and Chemistry of Minerals, 33, 639–650.
Sánchez-Muñoz, L., Correcher, V., García-Guinea, J., and Delgado, A. (2007) Luminescence at 400 and 440 nm in sanidine feldspar from original and X-ray-induced defects. Nuclear Instruments and Methods in Physic Research A, 580, 679–682.
Sánchez-Muñoz, L., García-Guinea, J., Zagorsky, V. Ye., Juwono, T., Modreski, P.J., Cremades, A., Van Tendeloo, G., and De Moura, O.J.M. (2012) The evolution of twin patterns in perthitic K-feldspar from granitic pegmatites. The Canadian Mineralogist, 50, 989–1024.
Scambos, T.A., Smyth, R.J., and McCormick, T.C. (1987) Crystal-structure refinement of high sanidine from the upper mantle. American Mineralogist, 72, 973–978.
Schröder, K.P., and Sauer, J. (1993) Preferred stability of the Al-O-Si-O-Al linkages in high-silica zeolite catalysts. Theoretical predictions contrary to Dempsey's rule. The Journal of Physical Chemistry, 97, 6579–6581.
Sherriff, B.L., and Hartman, J.S. (1985) Solid-state high-resolution ^{29}Si NMR of feldspars: Al-Si disorder and the effect of paramagnetic centres. The Canadian Mineralogist, 23, 205–212.
Smith, J.V. (1954) A review of the Al-O and Si-O distances. Acta Crystallographica, 7, 479–483.
——— (1974) Feldspar minerals, 1, p. 423–436. Springer Verlag, New York.
Smith, J.V., Blackwell, C.S., and Hovis, G.L. (1984) NMR of albite microcline series. Nature, 309, 140–142.
Stebbins, J.F., Du, L.S., Kroeker, S., Neuhoff, P., Rice, D., Frye, J., and Jakobsen, H.J. (2002) New opportunities for high-resolution solid-state NMR spectroscopy of oxide materials at 21.1- and 18.8-T fields. Solid State Nuclear Magnetic Resonance, 21, 105–115.
Taylor, W.H. (1933) The structure of sanidine and other feldspars. Zeitschrift für Kristallographie, 85, 425–442.
——— (1965) Framework silicates: The feldspars. In W.L. Bragg and G.F. Claringbull, Eds., Crystal Structures of Minerals, chap. 14, 293–339. G. Bell and Sons, London, U.K.
Taylor, W.H., Darbyshire, J.A., and Strunz, H. (1934) An X-ray investigation of the feldspars. Zeitschrift für Kristallographie, 87, 464–498.
Welberry, T.R. (2004) Diffuse X-ray scattering and models of disorder. IUCr Monographs on Crystallography 16, Oxford University Press, U.K.
Winter, J.K., Okamura, F.P., and Ghose, S. (1979) A high-temperature structural study of high albite, monalbite, and the analbite→monalbite phase transition. American Mineralogist, 64, 409–423.
Xiao, Y., Kirkpatrick, R.J., Hay, R.L., Kim, Y.J., and Phillips, B.L. (1995) Investigation of Al, Si order in K-feldspars using ^{27}Al and ^{29}Si MAS NMR. Mineralogical Magazine, 59, 47–61.
Zhou, L., Guo, J., Yuan, H., and Li, L. (1994) Solid state nuclear magnetic resonance and infrared spectroscopy of alkali feldspars. Science in China (Series D), 40, 2, 159–165.
Zhou, L. Guo, J., Liu, B., and Li, L. (2001) Structural state of adularia from Hishikari, Japan. Chinese Science Bulletin, 46, 950–953.

Manuscript received December 21, 2012
Manuscript accepted July 25, 2013
Manuscript handled by Brian Phillips